Research Square

Preprints are preliminary reports that have not undergone peer review.
They should not be considered conclusive, used to inform clinical practice,
or referenced by the media as validated information.

Assessing thermostable peroxygenase cytochrome P450 enzymes as biocatalysts for selective oxidations

Oghenesivwe Osiebe
Adelaide University
Daniel Z. Doherty
Adelaide University
Stephen G. Bell
stephen.bell@adelaide.edu.au
Adelaide University

Research Article

Keywords: Biocatalysis, C-H bond activation Heme enzymes, Oxidation, Peroxygenases, Protein Engineering

Posted Date: November 19th, 2026

DOI: https://doi.org/10.21203/rs.3.rs-11416052/v1

License: This work is licensed under a Creative Commons Attribution 4.0 International License.
Read Full License

Additional Declarations: Competing interest reported. S.G.B. is an inventor on a patent related to this work (PCT/AU2024/050934 and WO2025/043300).

Assessing thermostable peroxygenase cytochrome P450 enzymes as biocatalysts for selective oxidations

Oghenesivwe Osiebe, Daniel Z. Doherty and Stephen G. Bell

Discipline of Chemistry, School of Physics, Chemistry and Earth Sciences, Adelaide University, Adelaide, SA 5005, Australia

E-mail: stephen.bell@adelaide.edu.au

Author Contribution

Stephen G. Bell conceptualized the study and all contributed to its design. Protein purification and all analysis and experimental work was done by Oghenesivwe Osiebe, with training and assistance from Daniel Z Dohertry and Stephen G. Bell. The first draft of the manuscript and the revisions were written by Oghenesivwe Osiebe with assistance from Stephen G. Bell. All authors read and approved the final manuscript.

Abstract

Cytochrome P450 monooxygenases (CYPs) are promising biocatalysts for synthetic applications which are under-exploited, in part, due to their reliance on electron transfer proteins, high-cost nicotinamide cofactors and low stability. Here we report the engineering of peroxygenase functionality into three CYPs, CYP154H1, CYP154G1 and CYP154F1, from the thermophilic bacterium *Thermobifida fusca* XY. We introduced glutamine and glutamate residues at the conserved acid and alcohol residues involved in oxygen activation within the I-helix of CYPs. These enzymes catalysed distinct substrate bioconversions, compared to steroid oxidising CYP154C enzymes, when supported by H_2O_2. Across the three enzymes they catalysed the oxidation of indole, and the epoxidation of styrene, the hydroxylation of ethylbenzene and the sulfoxidation of thioanisole with CYP154H1 being the most active enzyme. CYP154F1 catalysed the terminal hydroxylation of geraniol but with low activity. CYP154G1 and CYP154H1 were more active for geraniol oxidation and generated a more complex mixture of aldehydes, epoxides, and oxygenated metabolites from terminal and subterminal oxidations. We demonstrate that the enantioselectivity of the engineered CYP154H1 in styrene, ethylbenzene and thioanisole oxidation reactions is improved compared to that reported for the wild-type enzyme. Mechanistic studies with isotopically labelled H_2O_2 and antioxidants demonstrate that the peroxide was the source of the oxygen in the initial product metabolites. All three enzymes were resistant to heat denaturation having melting temperatures of 60-71 °C. The best enzyme/substrate combinations generated product with an excess of 1300 total turnovers. This demonstrates that these new-to-nature peroxygenases can function as robust biocatalysts for oxidation reactions.

Keywords

Biocatalysis; C-H bond activation Heme enzymes; Oxidation; Peroxygenases; Protein Engineering

Introduction

Cytochrome P450 monooxygenases (CYPs or P450s) is a superfamily of hemoproteins known to perform various oxidation reactions including hydroxylations and epoxidations [1-4]. This superfamily is a versatile collection of natural biocatalysts for these and other oxidation reactions with immense potential for synthetic chemistry due to their ability to act on inert C-H bonds with high selectivity [5-7]. Across the superfamily, they catalyse the biotransformation of a wide range of organic substrates and have been explored for the synthesis of a diverse array of fine chemicals including pharmaceuticals and flavours and fragrances [8-14]. The demand for fine chemicals is continually increasing and enzymes are promising agents for developing more environmentally friendly synthetic approaches [15, 16]. The use of enzyme catalysts in synthesis offers advantages over traditional methods due to their high substrate specificity, product selectivity, mild reaction conditions and they can facilitate a reduction in step count [17, 18]. Despite the potential of CYPs, their industrial application is limited due to their reliance on additional electron transfer proteins and high-cost nicotinamide cofactors, as well as their low stability to non-biological conditions [19-21].

Several methods have been reported for the conversion of CYP monooxygenases into peroxygenases through protein engineering [22-27]. One approach is to mutate specific regions in the oxygen binding groove of the I-helix [7, 18, 28-30]. This approach replaces highly conserved acid-alcohol residues within the I-helix above the heme in CYP monooxygenases with residues capable of acid-base chemistry [30-32]. This switch from monooxygenase to peroxygenase function can be induced in a selection of CYPs by converting these acid and alcohol residues (or equivalents) to a glutamine and glutamate, respectively (QE double mutant) [7, 18, 29]. These QE variants introduce residues within the oxygen binding groove that mimic that of the natural peroxygenases of the CYP255 family, which are involved in the O-demethylation of lignin-derived aromatics [32-35]. This method has been demonstrated to

be successful for a small selection of CYP enzymes including individual members of the CYP199, CYP102, CYP107, CYP1579 and CYP154 families [28, 29, 36, 37]. However the general nature and role of this modification across multiple CYP enzymes to generate more efficient peroxygenase biocatalysts needs to be confirmed to expand the oxidation of more diverse substrates.

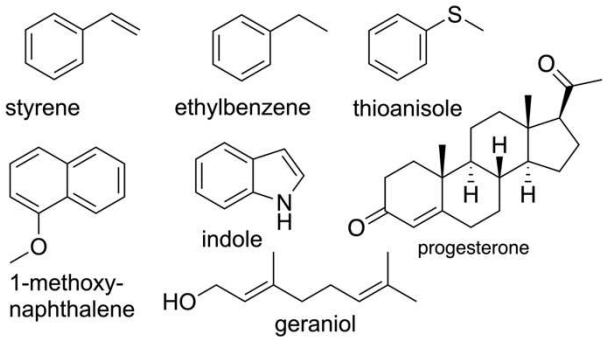
The bacterial CYP154 family of heme monooxygenases is commonly found in Actinobacteria [38, 39]. Currently, in the P450-Atlas database, forty CYP154 subfamilies have been identified and these contain over 600 unique sequences making up 242 ortholog groups, suggesting that these may be able to facilitate varied oxidative biotransformations. However, to date only a few CYP154 enzymes have been characterised [39]. Known CYP154 enzymes can perform a range of chemical rearrangements on a versatile range of substrates including the oxidation of steroid, aromatics terpenes and fatty acids [40-43]. For example, the CYP154C subfamily member enzymes mainly oxidise steroids; including CYP154C5 and CYP154C35 from *Nocardia* species, CYP154C3, CYP154C7, and CYP154C8 from *Streptomyces* species, among others [36, 44-47]. An unusual reaction, the cycloaddition of dipentaenone, is catalysed by CYP154A1 from *Streptomyces coelicolor* [48]. CYP154A8 from *Nocardia farcinica*, catalyses the hydroxylation of linear medium-chain alkanes (C7-C10) [49]. CYP154H1 from *Thermobifida fusca* XY catalyses the oxidation of styrene, ethylbenzene, indole, thioanisole and 1-octene [50]. CYP154E1 from the same bacterium is reported to catalyse the bioconversion of a wide range of substrates including geraniol and nerol [40]. CYP154F1, also from *T. fusca*, is reported to have a narrower substrate range than CYP154E1 and catalyses the hydroxylation of geraniol and octanoic acid [51]. The diverse substrate range observed within these CYP154 family members make them good targets for further study for biocatalytic applications. The majority of the reported reactions are supported using the enzyme's monooxygenase pathway and used non-physiological redox partner proteins and nicotinamide

cofactors. The concentration of the redox partner proteins used in these reactions is normally significantly higher than that of the of the CYP enzyme (often 10-fold) and this can limit their practical use [52, 53].

Several of these CYP154 enzymes are found in thermostable bacteria. The ability of proteins to resist temperature denaturation and maintain optimal activity over a broad range of temperatures for a significant period of time is a desirable property in biocatalysis, however, the majority of studied CYPs are from mesophiles and these, and their electron transfer partner proteins, denature at moderate temperatures and require cryostorage [54, 55]. Therefore, thermophilic bacteria have been explored as a source of proteins, and recently, a number of thermostable CYPs have been characterised [29, 50, 56-59]. *T. fusca* XY is a thermostable actinobacterium with optimum growth temperature between 50-55 ℃ [41, 60-62]. Previously, cellulolytic enzymes from strains of this bacterium have been found to be thermostable [63]. Schallmey and coworkers, reported that CYP154H1 from the bacterium retained 54% of its initial activity after heating for 10 min at 65 ℃, with a melting temperature of 67 ℃ [50]. *T. fusca* XY contains ten CYP encoding genes, including four CYP154 enzymes from the E, F, G and H subfamilies [64]. Of these, the monooxygenase activities of wild-type (WT) CYP154H1, CYP154F1 and CYP154E1 enzymes have been studied [40, 50, 51]. The activity of WT CYP154H1 has been previously reconstituted with NADH and the heterologous redox partners, putidaredoxin reductase (Pdr) and putidaredoxin (Pdx) [50]. Investigation of the CYP154G1 enzyme from this bacterium is yet to be reported.

Here, we focus on developing peroxygenase biocatalysts from the H, F and G subfamilies of the CYP154 family which are thermostable. We explore three CYPs, CYP154H1, CYP154F1 and CYP154G1 from the thermophilic bacterium *T. fusca* XY and compare these to a member of the CYP154C subfamily, CYP154C35 which has previously been converted and used as a peroxygenase [36]. We convert these enzymes from monooxygenases to peroxygenases

through modification of the I-helix sequence and report the activity for a selection of substrates and determine the thermostability of the mutant forms of these enzymes [36]. To cross compare the enzyme activity, we tested the QE mutants of the CYP154 enzymes using H_2O_2 supported reactions with substrates (styrene, ethylbenzene and thioanisole) that have previously been shown to be oxidised by CYP154H1 (Scheme 1). The enzymes were also tested with geraniol which is the best substrate reported for CYP154F1 and progesterone, which is oxidised by CYP154C subfamily enzymes [36, 51]. Additionally, we tested the potential of the enzymes to catalyse aromatic oxidations using indole and 1-methoxynaphthalene, which can generate coloured metabolites, as substrates (Scheme 1).



Scheme 1. Structures of compounds used in this study to characterise peroxygenase activity of the CYP154 enzymes.

Experimental Methods

General

The codon-optimised genes of the QE mutants, CYP154H1QE, CYP154G1QE, CYP154F1QE and the WT CYP154H1 and CYP154F1 were obtained in pET28a plasmid constructs, which were purchased from Twist Bioscience (USA). WT and QE mutant of CYP154C35 were obtained previously [36]. Competent BL21 (DE3) *E. coli* cells were from New England Biolabs. Styrene, ethylbenzene, thioanisole, geraniol, progesterone, bovine catalase and ethyl acetate were sourced from Sigma-Aldrich. Pyridine and HPLC grade acetonitrile was from Ajax Finechem (Thermo Fisher Scientific).

The products of the enzyme reactions were analysed by a combination of GC-MS, enantioselective GC, HPLC and UV-Visible spectrophotometry. GC-MS analysis was done using a Shimadzu GC-2010 coupled to a GC-MS-QP2010S detector equipped with an Agilent DB-5 MS fused silica column (30 m x 0.25 mm x 0.25 μm). Enantioselective GC analysis was carried out using a Shimadzu Tracera GC coupled to Barrier Discharge Ionization Detector (BID) equipped with a RT® - BDEXse chiral silica column (CP-Chirasil; 25 m x 0.32 mm x 0.25 μm). For HPLC analysis, we utilised a Shimadzu LC-20AD HPLC system, equipped with a Phenomenex Kinetex 5μm XB-C18 reversed-phase liquid chromatography column (250 × 4.6 mm, 5 μm), SIL-20 A autosampler, CTO-20 A, SPD20A UV detector and CBM-20A lite communications module. UV-Vis absorbance spectrophotometry was performed using a Cary 60 UV-Vis spectrophotometer (Agilent Technologies) coupled to a Peltier unit to maintain the temperature at 30 °C. Samples in quartz cuvettes with a 1 cm path length were scanned at 600 nm min^{-1}.

Production of the WT CYP154H1, CYP154H1QE, CYP154FQE and CYP154G1QE enzymes

The pET28 plasmids containing the CYP genes (1 μL of plasmid DNA; 150-250 ng/μL) were added to 20 μL competent BL21 (DE3) *E. coli* (C2527) cells and kept on ice for 45 min. The

mixture was transferred to a heat block at 42 ℃ for 45 s (heat shock) and immediately cooled on ice for 2 min. After cooling, 200 µL of prewarmed and sterile SOC media (Super Optimal broth with catabolite repression) was added to the mixture, and these were incubated for 2 h at 37 ℃ and 150 rpm. Cells were subsequently plated on LB (Lennox) agar medium (containing 5 g of Bacto yeast extract, 5 g of sodium chloride, 15 g of agar and 10 g of Bacto tryptone in 1 L) containing 30 µg/mL kanamycin and incubated at 37 ℃ for 16-18 h to obtain bacterial colonies.

Proteins were produced by transferring colonies from the LB agar plates into LB broth media (3×750 mL) containing 30 µg/mL kanamycin. The cells were grown at 37 ℃ and 120 rpm for ~8 h. At the end of this period, the temperature and shaking speed were reduced to 28 ℃ and 100 rpm respectively before addition of 2% v/v ethanol and 0.02% v/v benzyl alcohol [65, 66]. The cultures were incubated at the same temperature for 30 min before inducing protein expression by addition of 20 µM isopropyl-β-D-1-thiogalactopyranoside (IPTG). The bacterial cultures were grown at 28 ℃ and 100 rpm for 48 h. Bacterial cells were harvested by centrifugation for 10 min at 5,000 g and 4 ℃, and the cell pellets were stored at -20 ℃ prior to protein extraction.

Enzyme extraction and purification

Frozen cell pellets were thawed and resuspended in 200 mL of 50 mM Tris-HCl buffer pH 7.4. Cell lysis was performed on ice by sonication using a Vibra-Cell VC 505 ultrasonic processor (Sonics & Materials, USA) with a CV334 probe (70% amplitude, pulse of 10 s and cycle interval of 50 s) and manual stirring at intervals to prevent overheating. Centrifugation for 20 min at 39,000 *g* and 4 ℃ was used to remove cell debris and insoluble matter from the protein containing lysate. The clarified supernatant containing the crude protein was loaded onto three His-Trap (Protino Ni-NTA) 5 mL columns in series for purification by nickel-histidine affinity chromatography. The column was equilibrated with five column volumes of binding buffer (20

mM sodium phosphate buffer pH 7.4, containing 0.5 M NaCl and 20 mM imidazole). Crude protein was loaded on the column at a flow rate of 2-3 mL min^{-1}. After the protein was loaded, the column was washed with five column volumes of binding buffer. The bound CYP protein was eluted at 2 mL min^{-1} using elution buffer (20 mM sodium phosphate buffer pH 7.4, containing 0.5 M NaCl and 200 mM imidazole) and the red-coloured eluent was collected. Eluted proteins were concentrated by ultrafiltration using a 10 kDa exclusion membrane (Sartorius) and desalted on Sephadex G-25 coarse grain column with 50 mM Tris-HCl buffer pH 7.4. The proteins were purified via anion-exchange chromatography using DEAE Fast Flow Sepharose anion-exchange column (XK 50, 200 × 40 mm; GE Healthcare) and eluted with a gradient of 0-600 mM KCl. Collected fractions containing CYPs were combined and concentrated by ultrafiltration using Sartorius 10 kDa filtration membrane before desalting on Sephadex G-25 coarse grain column, with 50 mM Tris-HCl buffer pH 7.4, concentrated and stored. Proteins were stored in 40-50% v/v autoclaved glycerol at -20 ℃. Before each experiment, the glycerol was removed by PD-10 gel filtration chromatographic column (Cytiva) into 50 mM Tris-HCl buffer pH 7.4.

Sodium dodecyl sulfate-polyacrylamide gel electrophoresis (SDS-PAGE) analysis

The purified proteins were analysed by SDS-PAGE using precast gels (4-12%) from GenScript Incorporated (USA). Electrophoresis was performed at 110 V for 20 min for protein stacking, followed by 150 V for 40 min. Gels were visualised using Coomassie Brilliant Blue R250 stain (0.1% Coomassie Brilliant Blue R250, 50% methanol and 10% glacial acetic acid) for 1 h and destained using milli-Q water with gentle rocking until bands were clearly visible [67].

UV-Vis absorbance analysis

The UV-Vis absorbance spectra of the CYPs were recorded between 250-700 nm. Substrate binding analysis were done with ~2 μM of enzyme and 1 mM substrate. Binding experiments with 1-methoxynaphthalene contained 0.2 mM substrate.

For CO assays, the instrument was baselined with 50 mM Tris-HCl buffer pH 7.4. Each enzyme was diluted in buffer to have a Soret band absorbance of ~0.5-0.6 and the spectrum was recorded. A few grains of sodium dithionite (< 1 mg) were then added to reduce the enzyme, and the ferrous spectrum was recorded. Carbon monoxide (CO) was then gently bubbled into the reduced enzyme solution through a syringe needle for ~10 s to generate the ferrous P450-CO adduct and the UV-Vis absorbance spectrum was recorded.

The ε_{Soret} of each CYP was determined by the pyridine hemochromogen method [68]. The enzyme was diluted until the Soret band absorbance was between 1-1.6 in 50 mM Tris-HCl buffer, pH 7.4 and the ferric spectrum was recorded. The instrument was then baselined with a 1:1 mixture of Tris buffer and solution A (40% [v/v] C_5H_5N, 0.2 M NaOH, and 500 μM $K_3[Fe(CN)_6]$). An enzyme solution of 500 μL was added to 500 μL of solution A and the UV-Vis absorbance spectrum was recorded. To generate the reduced pyridine hemochromogen species, a few grains of sodium dithionite (< 1 mg) were added to the enzyme and the spectrum was recorded. The heme content was then quantified using ε_{556} = 34.7 mM^{-1} cm^{-1}. After heme quantification, the extinction coefficients of the Soret band for WT CYP154H1, CYP154H1QE, CYP154G1QE, and CYP154F1QE were calculated using Beer's equation [68, 69].

H_2O_2 Heme bleaching

To observe the rate at which heme bleaching occurs, each enzyme was mixed with H_2O_2 and monitored by UV-Vis absorbance spectrophotometry. The reaction mixture contained 2 μM of the respective enzymes in 50 mM Tris-HCl buffer pH 7.4 and 10 mM H_2O_2. Heme bleaching

was monitored in the absence or presence of 1 mM styrene (CYP154H1QE, WT CYP154H1 and CYP154G1QE) or geraniol (for CYP154F1QE). The spectrum of the reaction mixture was recorded at 0 min and then at 2 or 5-min intervals for 10-25 min.

In vitro H_2O_2-driven oxidation reactions

All reactions were conducted in in Tris-HCl buffer pH 7.4. The reaction mixture contained 3 μM of enzyme, 5-10 mM H_2O_2 and 10 mM substrate (styrene and ethylbenzene) or 0.5 mM substrate (geraniol). Reactions with thioanisole contained 3 μM of enzyme, 1 mM substrate and 1 mM H_2O_2. Reactions with indole and 1-methoxynaphthalene contained 1 μM enzyme, 5-10 mM H_2O_2 and 1 mM of respective substrates. Progesterone oxidation reactions contained 1 μM of the respective enzymes, 500 μM substrate and 10 mM H_2O_2. The reactions were incubated in a shaking incubator at 25 ℃ and 120 rpm. Negative control reactions were carried out under identical conditions without the addition of the enzyme.

In vitro oxidation reactions with labelled $H_2{}^{18}O_2$

The reactions contained 3 μM (CYP154F1QE or CYP154G1QE) or 1 μM CYP154H1QE, 1 mM indole and 2 mM $H_2{}^{18}O_2$ for 3 h. With styrene and ethylbenzene, the mixtures contained 3 μM of CYP154H1QE, 10 mM substrate and 2 mM $H_2{}^{18}O_2$ for 3 h. Reactions with thioanisole contained 3 μM of CYP154H1QE, 1 mM substrate and 1 mM isotopically labelled $H_2{}^{18}O_2$. Reactions with 1-methoxynaphthalene contained 1 μM CYP154H1QE, 2 mM $H_2{}^{18}O_2$. and 1 mM substrate. Geraniol oxidation reactions contained 1 μM CYP154H1QE, 500 μM substrate and 2 mM $H_2{}^{18}O_2$. The reactions were incubated in a shaking incubator at 25 ℃ and 120 rpm. Negative control reactions were carried out under identical conditions without the addition of the enzyme. Positive control reactions were carried out in identical conditions with non-labelled H_2O_2.

Reactions were set up as above using H_2O_2 in the presence or absence of 2 mM ascorbic acid.

Determination of thermostability

The thermostability of the enzymes was determined by measuring the residual enzyme activity after incubation at elevated temperatures. Enzymes in 50 mM Tris-HCl buffer pH 7.4 were incubated in a heat block for 1 h between 45-80 °C and oxidation reactions were then carried out as described above. Reactions contained 3 μM enzyme, in Tris-HCl buffer pH 7.4, 10 mM styrene and 5 mM H_2O_2 (CYP154F1QE) or 10 mM H_2O_2 (CYP154H1QE and CYP154G1QE). The enzyme activity was measured using the quantity of styrene oxide formed after incubation at each temperature. The activity of the unincubated enzyme was defined as 100%, and the relative enzyme activity at respective temperatures was calculated. The data obtained was fitted into a Hill-type equation on GraphPad, and the line of best-fit and the corresponding T_{50} ($^{60}T_m$) were extracted. T_{50} was defined as the temperature at which the residual enzyme activity (y) is 50% of the initial activity (y_0).

$$y = y_0 - \frac{(y_0 \times T^h)}{(T_{50}^h + T^h)}$$

Metabolite analysis

To prepare reactions for HPLC analysis, 132 μL of the mixture was quenched with 1 μL of catalase (10 mg/mL stock solution) to remove any unused H_2O_2. Quenched reactions were mixed with 58 μL of acetonitrile and 2 μL of internal standard (10 mM 9-hydroxyfluorene) before centrifuging at 18,700 g for 2 min. For analysis, a gradient of 20-95% acetonitrile in water (with 0.1% TFA) over a period of 30 min was used for sample elution at a flow rate of 1 mL min^{-1}, and the eluate was monitored at 254 nm. To confirm the identity of the products, available standards were analysed under the same conditions.

For GC-MS and GC analysis, 600 μL of the reaction mixture was quenched with 1 μl of 10 mg/ml catalase, before addition of 6 μl of 10 mM 9-hydroxyfluorene. The organic component of the mixture was extracted using 300 μL of ethyl acetate before isolation and analysis.

The GC-MS ion source and interface temperatures were set to 250 ℃ and 280 ℃, respectively. The oven temperature was held at 60 ℃ for 3 min before heating at 10 ℃ min^{-1} up to 140 ℃ and then held for 5 min. The oven temperature was heated at 40 ℃ min^{-1}, when the column reached 240 ℃, it was held for 1.5 min at this temperature. The products were initially identified by matching the mass spectra obtained to those in the NIST library and confirmed by matching the retention times with authentic product standards. This was followed by calibration with the product standards to determine the concentration of the metabolites from the enzyme catalysed reactions.

UV-Vis absorbance spectrophotometry was used to analyse colorimetric reactions with indole and 1-methoxynaphthalene. The instrument was first baselined with 50 mM Tris-HCl buffer pH 7.4, between 250-800 nm at 300 nm min^{-1} before analysis. The amount of 4,4-dimethoxy-1,4-diphenylbutane-1,3-dione (Russig's blue) formed from 1-methoxynaphthalene oxidation was quantified using $\varepsilon_{610} = 1.45 \times 10^4$ M^{-1} cm^{-1} [70-72].

Results and Discussion

Production and spectroscopic characterisation of WT CYP154H1 and CYP154H1QE

To assess if the QE double mutant variants engender increased peroxygenase activity into the CYP154H1 enzyme as it does with the CYP154C subfamily, we first compared and assessed the activity of the WT and mutant forms of the enzyme [36]. Genes encoding WT CYP154H1 and CYP154H1QE enzymes were obtained in pET28a plasmid DNA constructs and used to produce the enzymes in *E. coli* (see supporting information for details of plasmid constructs). The proteins were purified using nickel affinity, desalting and anion exchange chromatography. After quantitation by UV-Vis absorbance spectrophotometry, we obtained 40 mg of purified CYP154H1QE per litre of media (Figure S1). In comparison, 85 mg per litre of WT CYP154H1 was obtained after purification (Figure S1).

The ferric resting states of CYP154H1QE and WT CYP154H1, had similar Soret band maximum absorption at 416 nm (Figure 1 and Figure S1). The purified CYP154H1QE and WT CYP154H1 had Reinheitszahl (R_Z) values of 1.1 and 1.6, respectively (Figure S1**)**. The lower R_Z value of CYP154H1QE in comparison to the WT CYP154H1 was in part due to its broader Soret band due to the presence of a shoulder at ~396 nm (Figure S1). SDS-PAGE analysis of the enzymes showed single bands corresponding to ~48.3 kDa for both the CYP154H1QE and the WT CYP154H1 enzymes (Figure S2), indicating that the enzymes were prepared to high purity (>95%).

After the reduction of the ferric enzymes with sodium dithionite, there was noticeable decrease in the Soret absorption peaks of CYP154H1QE and WT CYP154H1 at 416 nm (Figure 1). For both enzymes, addition of carbon monoxide resulted in the generation of split Soret band, comprising a peak at ~450 nm and ~420 nm (Figure 1). The peak at ~450 nm is due to the formation of the ferrous P450-CO adduct which is a characteristic property of these enzymes, indicating the successful production of a functional ferrous thiolate CO-bound protein [73].

The peak at ~420 nm is proposed to arise from a ferrous thiol species or potentially an inactive form of the CYP enzyme [74, 75].

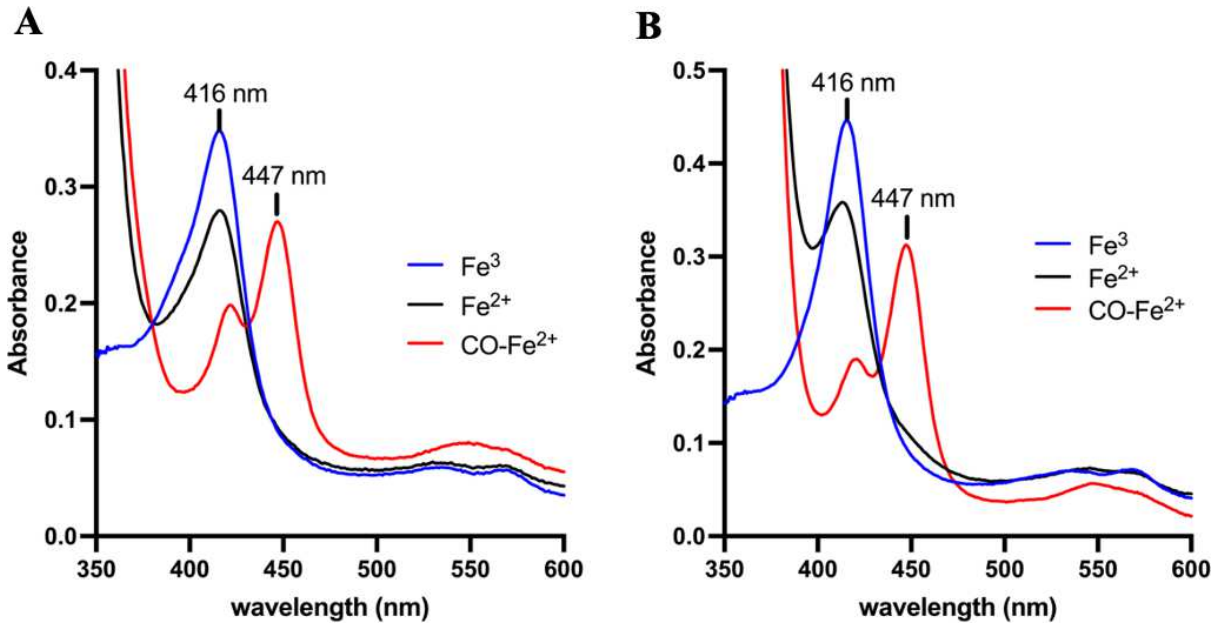


Fig. 1 UV-Vis absorbance spectra of the ferrous CO-bound complex of CYP154H1 from *T. fusca*. (**A**) CYP154H1QE, (**B**) WT CYP154H1. The ferric (blue), ferrous (black) and ferrous-CO-bound (red) spectra are shown

Consequently, the ε_{Soret} of the enzymes were determined using the pyridine hemochromogen method (Figure S3) [68]. The extinction coefficients of CYP154H1QE and WT CYP154H1 were calculated to be ε_{416} 108 ± 2 mM^{-1} cm^{-1}, and ε_{416} 129 ± 3 mM^{-1} cm^{-1}, respectively. To the best of our knowledge, the ε_{Soret} of the enzymes from *T. fusca* have not been previously reported, however, our results are similar to literature values reported for other CYPs [75, 76].

Comparison of the peroxygenase activity of CYP154H1 and CYP154C35 variants

To assess whether our two-point QE mutation increased peroxygenase activity we chose to study the activity of the CYP154H1 enzymes for H_2O_2 driven oxidation. To establish that the different CYP154 subfamilies are likely to work on different substrates and to assess the transferability of the method used to increase peroxygenase activity, we compared these

reactions to CYP154C35. We tested the oxidation of ethylbenzene as this is an established substrate for CYP154H1 and progesterone, an excellent substrate for CYP154C35 (Table 1, Figure 2, Figure S4) [50]. In ethylbenzene oxidation reactions with CYP154H1QE, we observed the formation of high levels of 1-phenylethanol (343 ± 40 μM) and 1-phenylethanone (101 ± 10 μM; acetophenone), a further oxidation metabolite. In reactions with WT CYP154H1 only 1-phenylethanol was formed and at much lower levels. The total turnover number (TON) was 7 ± 0.2 μM per μM of enzyme (Figure 2A and 2B). In comparison, CYP154H1QE variant generated a TON of ~545, a greater than 75-fold increase in peroxygenase activity over the WT enzyme. Progesterone oxidation supported by H_2O_2 with WT CYP154H1 and CYP154H1QE did not generate any detectable product [50]. In contrast to CYP154H1QE, the CYP154C35QE enzyme showed very low levels of product formation with ethylbenzene but completely converted progesterone into 16α-hydroxyprogesterone, with TON of ~1 and 500, respectively (Figure 2C and Table 1). Under identical conditions, reactions of WT CYP154C35 with progesterone did not generate any product [36].

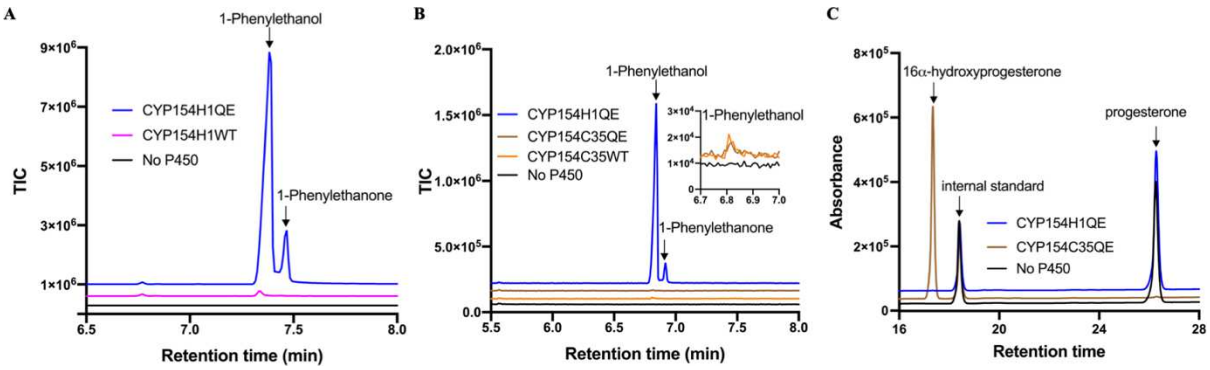


Fig. 2 GC-MS and HPLC chromatograms comparing the peroxygenase activity of CYP154 enzymes from the CYP154H and CYP154C subfamilies. Ethylbenzene reaction contained 3 μM of the respective enzymes in Tris-HCl buffer pH 7.4, 10 mM of ethylbenzene, and 10 mM H_2O_2 (maximum TON ~3330). The retention time of ethylbenzene was 3.44 min. Progesterone oxidation reactions contained 1 μM enzyme in Tris-HCl buffer pH 7.4, 500 μM substrate and 10 mM H_2O_2 (maximum TON 500). The insert in panel B shows the very low levels of 1-phenylethanol formed in the CYP154C35 enzymes

Table 1. Comparison of the peroxygenase activity of WT CYP154H1, CYP154H1QE and CYP154C35QE enzymes in ethylbenzene and progesterone oxidations. (-) Signifies no detectable metabolite or no reaction.

	Product generated per μM enzyme		Turnover number
	Ethylbenzene oxidation		
	1-phenyl ethanol (μM)	1-phenylethanone (μM)	
WT CYP154H1	7 ± 0.2	-	7 ± 0.2
CYP154H1QE	343 ± 40	101 ± 10	545 ± 50
CYP154C35QE	1 ± 0.1	-	1
	Progesterone oxidation		
	16α-hydroxyprogesterone		
WT CYP154C35	-		-
CYP154C35QE	500		500
CYP154H1QE	-		-

These results demonstrate that the QE double mutation significantly enhances the peroxygenase activity of both of the CYP154 enzymes from different subfamilies. This is similar to our previous reports on the effect of QE mutation on CYP154C35QE when compared to WT CYP154C35 [36]. Additionally, our results show that within the CYP154 family, members from different subfamilies may have different substrate specificities, despite sharing at least 40% sequence similarities highlighting their potential as useful biocatalysts.

Having affirmed the positive effect of the QE mutations for peroxygenase activity for both the CYP154 subfamilies and their different substrate preferences, we hypothesised that similar mutants of CYP154F1 and CYP154G1 could be used to investigate the potential substrate specificities within the CYP154 enzymes from *T. fusca* using H_2O_2 driven oxidation reactions.

Production and spectroscopic characterisation of CYP154F1QE and CYP154G1QE

Genes encoding the variant CYP154F1QE and CYP154G1QE enzymes, obtained in pET28a plasmid DNA constructs (details in SI), were produced in *E. coli* and purified in three steps, following the same methods used for the CYP154H1 enzymes. After purification and

quantitation using UV-Vis absorbance spectrophotometry, we obtained 22 mg and 68 mg of CYP154F1QE and CYP154G1QE, respectively, per litre of media (Figure S1).

The ferric resting states of CYP154G1QE, and CYP154F1QE had Soret band absorbance maxima absorption at 417 nm and 419 nm respectively, (Figure S1 and Figure S3). The purified enzymes, CYP154G1QE and CYP154F1QE both had R_Z values of ~2.1 (Figure S1). SDS-PAGE analysis of the enzymes showed single bands corresponding to ~47.3 kDa, CYP154F1QE and ~45.9 kDa, CYP154G1QE **(**Figure S2). This indicates that the mutant enzymes, similar to CYP15H1QE and WT CYP154H1, were prepared to high purity.

On reduction of the ferric CYP154G1QE and CYP154F1QE enzymes by the addition of sodium dithionite, we observed little or no change in the spectra of the enzymes, in contrast to that of the CYP154H1 mutant and its wild-type form (Figure S5). When carbon monoxide was introduced into the reduced enzyme mixtures, split Soret bands comprising a peak at ~450 nm and ~420 nm was generated, similar to the CYP154H1 enzyme (Figure S5).

The ε_{Soret} of CYP154G1QE and CYP154F1QE were calculated using the pyridine hemochromagen method and were ε_{417} 120 ± 4 $mM^{-1}\,cm^{-1}$ and ε_{419} 130 ± 1 $mM^{-1}\,cm^{-1}$, respectively (Figure S3). These were similar to those of WT CYP154H1 and other CYPs [75, 76].

Substrate binding and heme bleaching assays

We performed substrate binding experiments with a range of compounds known to be oxidised by WT CYP154H1 and WT CYP154F1, to assess if there are substrate induced spectral changes, indicative of ligand binding within the active site [77, 78]. as is clearly observed for the binding of progesterone to CYP154C35QE [36]. The addition of the substrates did not result in significant shifts in the UV-Vis absorbance spectra of the *T. fusca* enzymes with a few exceptions (Figure S6-S9). With CYP154G1QE and styrene, the substrate induced a change corresponding to ~15% spin state shift from 419 nm (low spin) to 392 nm (high spin) in the

enzyme's spectrum (Figure 3A). Addition of geraniol to CYP154F1QE resulted in a small change in the UV spectrum of the enzyme corresponding to < 5% shift in the spin-state of the enzyme (Figure S9). A larger shift was observed with the addition of geraniol to CYP154G1QE (Figure 3B) corresponding to ~30% shift from the low spin to the high spin ferric state. Addition of geraniol to CYP154H1QE resulted in an ~1-2 nm red shift in the Soret band, indicative of a potential interaction with the alcohol moiety (Figure S9). We did not observe a significant change in the UV-Vis absorbance spectrum of CYP154H1QE on addition of styrene (Figure S6A). With WT CYP154H1, styrene induced a small blue shift in the Soret band from ~416 to 415 nm and an ~15% shift from the low spin to high spin (Figure S6B). Overall, the substrate binding results suggest that the sixth aqua ligand of the heme is not readily displaced by these substrates when they are added to the enzyme.

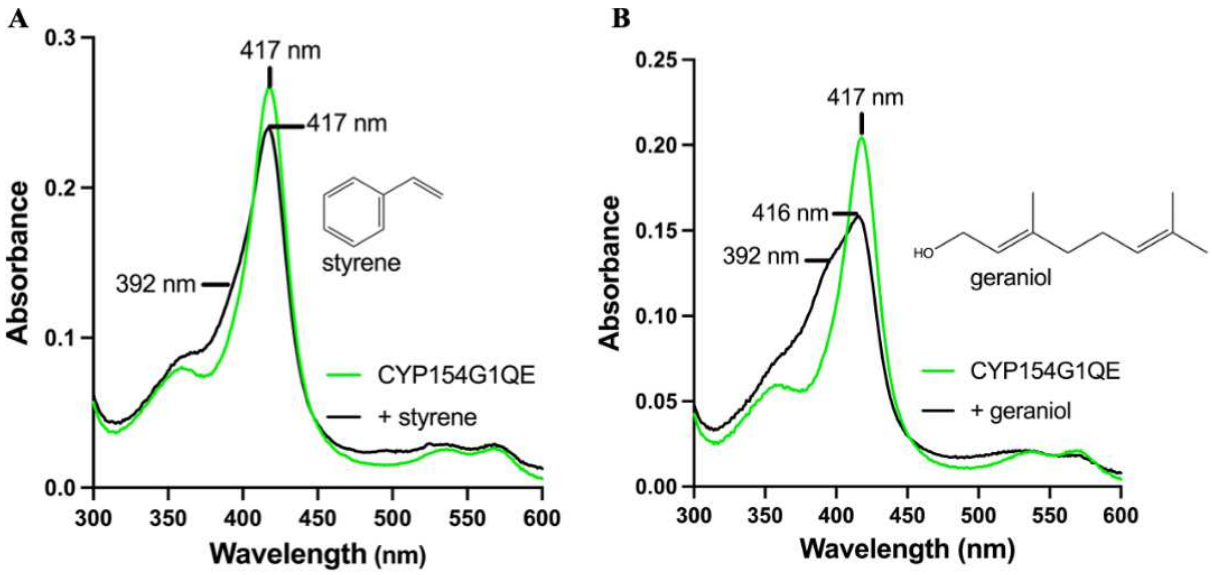


Fig. 3 UV-Vis absorbance spectra of CYP154G1QE (2 μM) before and after addition of substrates (1 mM). CYP154G1QE (green) (**A**) with styrene and (**B**) with geraniol; the substrate-bound enzyme (black)

Reactive oxygen species including hydrogen peroxide are known to inactivate CYPs through heme degradation or oxidation of the heme-bound cysteine ligand to sulfenic acid [79, 80]. Therefore, we investigated the stability of the engineered CYPs, to hydrogen peroxide which

would be used to drive the oxidation reactions. When using 10 mM H_2O_2, we observed heme bleaching rates increased in the order CYP154F1QE < CYP154H1QE < CYP154G1QE (Figure 4, Figure S10, Tables S1-S2).

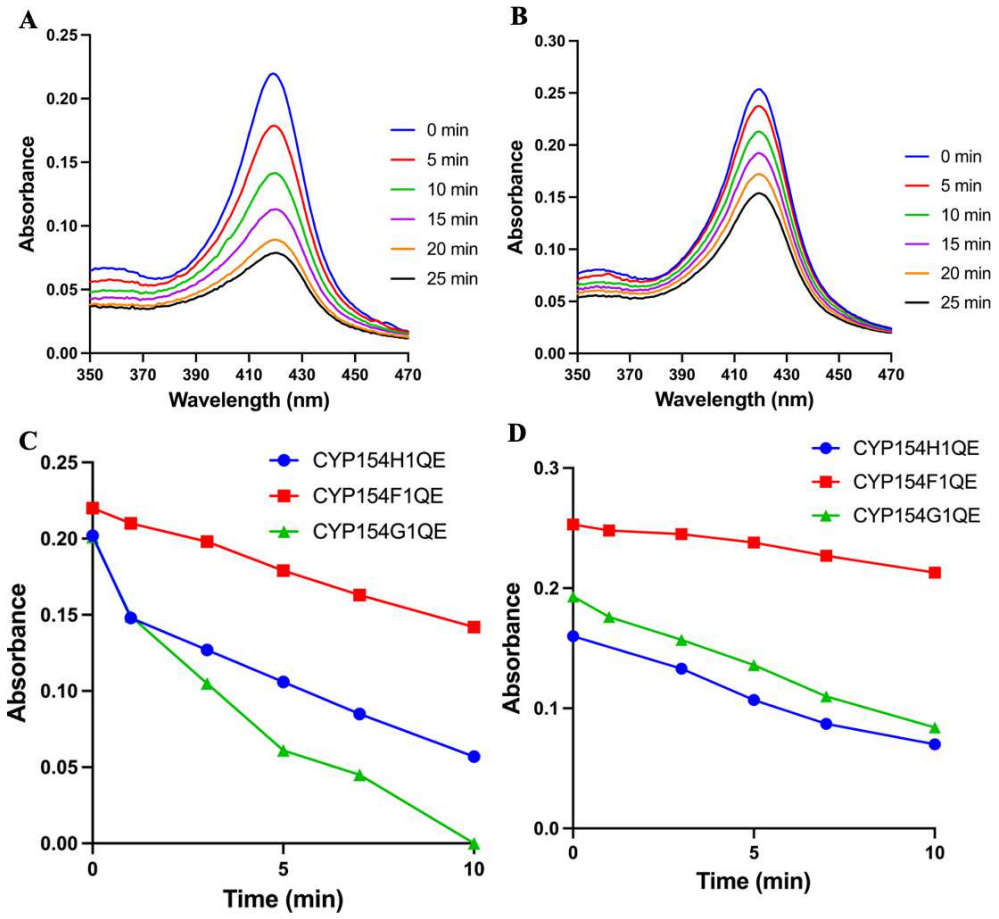


Fig. 4 Heme bleaching experiments of CYPs with H_2O_2 in the presence and absence of substrate (styrene or geraniol). (**A**) The UV-Vis absorbance of CYP154F1QE (2 µM) and 10 mM H_2O_2 in the absence of substrate and (**B**) in the presence of 1 mM geraniol. (**C**) The initial rates of heme bleaching of CYP154H1QE, CYP154F1QE and CYP154G1QE in the absence of a substrate and (**D**) presence of either 1 mM geraniol (CYP154F1QE), or 1 mM styrene (CYP154H1QE and CYP154G1QE)

CYP154H1QE showed a similar rate of heme bleaching to WT CYP154H1 in the presence of 1 mM styrene, however, without substrate, it was more rapidly bleached than the WT enzyme (Tables S1-S2). The heme bleaching rate of the three mutant CYP154 enzymes was between 0.06 – 0.12 µm min^{-1} without substrate (Table S2). The addition of a potential substrate ligand

(1 mM styrene or 1 mM geraniol) slowed the rate of heme bleaching in each instance by 2-fold to 0.032 – 0.074 μm min^{-1} (Table S1-S2). These results are consistent with previous observations that heme bleaching is slower in the presence of substrate [7, 29, 36]. The oxidation of the substrate can provide a pathway to protect the heme from degradation from the build-up of reactive intermediates, or the substrate could prevent excess H_2O_2 accessing regions of the heme that could result in adverse side reactions.

H_2O_2-driven oxidation reactions of styrene, ethylbenzene and thioanisole

Reactions were undertaken with the three mutant enzymes and a selection of substrates (Scheme 1). These were analysed and quantitated by GC-MS and/or HPLC (Figure S11-S15). Similar to CYP154H1QE, the mutant CYP154F1QE, catalysed the benzylic oxidation of ethylbenzene to 1-phenylethanol (Figures S4 and S16). However, the enzyme generated a significantly lower amount of 1-phenylethanol (0.2 μM of per μM of enzyme), with no detectable 1-phenylethanone (Tables 2, Figures S4 and S16). The CYP154G1QE enzyme did not generate any product with ethylbenzene.

Table 2. The amount of product generated per μM of enzyme (TON) in the oxidation of styrene, ethylbenzene and thioanisole oxidation.

	Styrene	**Thioanisole**	**Ethylbenzene**	
	Styrene oxide (μM)	Methyl phenyl sulfoxide (μM)	1-phenyl ethanol (μM)	1-phenyl-ethanone (μM)
CYP154H1QE	392 ± 3	90 ± 20	343 ± 40	101 ± 10
CYP154G1QE	18 ± 2	41 ± 2	-	-
CYP154F1QE	0.3 ± 0.04	-	0.23 ± 0.03	-

All three mutant enzymes CYP154H1QE, CYP154G1QE and CYP154F1QE catalysed the epoxidation of styrene to styrene oxide (Figure 5A, Table S3 and Figure S17). In addition to styrene oxide, the mutant enzymes also generated quantities of benzaldehyde and phenylacetaldehyde as minor products totalling between 0.4%-15% and 2.6%-8%, respectively

(Figure 5A and Table S3) [81, 82]. In these reactions, the total quantity of products formed by the enzymes was CYP154H1QE > CYP154G1QE > CYP154F1QE. The amount of styrene oxide formed was 392, 18, and 0.3 μM per μM enzyme, for CYP154H1QE, CYP154G1QE and CYP154F1QE, respectively (Table 2). WT CYP154H1 and CYP154C3QE generated 6 ± 0.1 and 10 ± 4 μM of styrene oxide per μM enzyme, respectively (Figure S18).

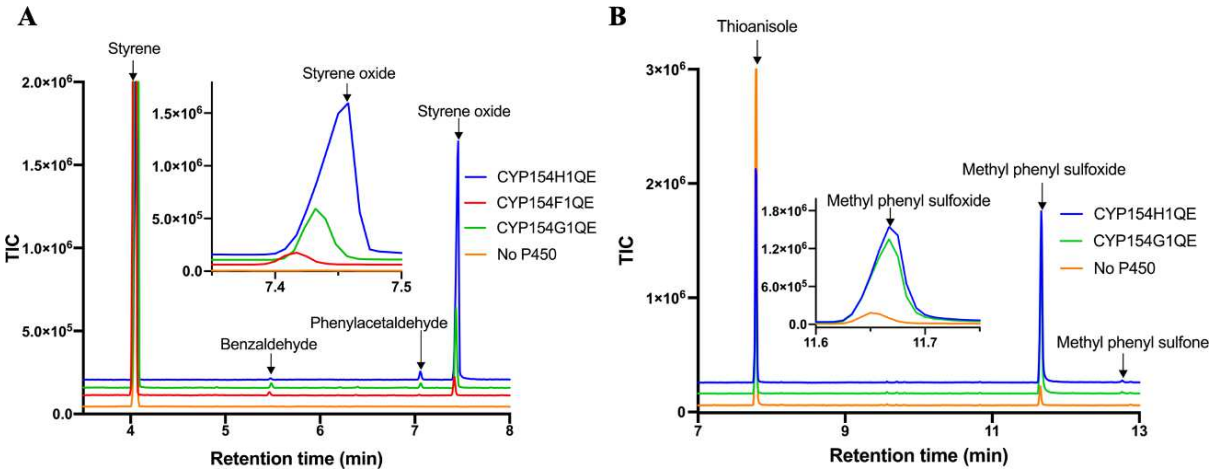
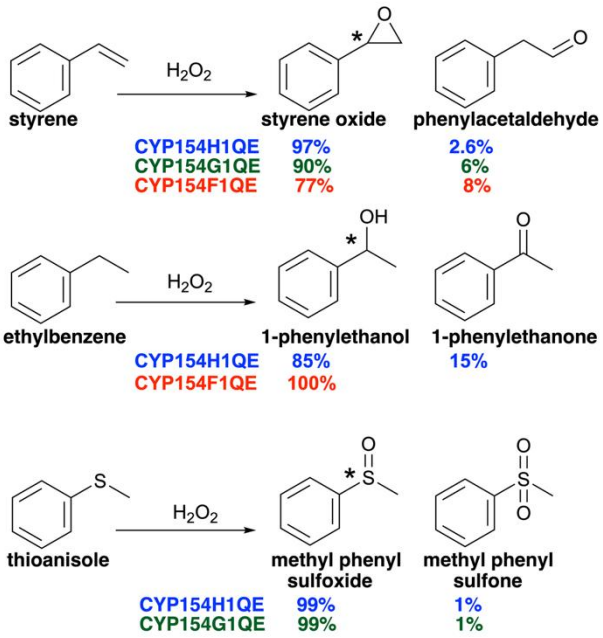


Fig. 5 GC-MS analysis of (**A**) styrene and (**B**) thioanisole oxidation using CYPs from *T. fusca*. Styrene oxidation reactions contained 1 μM enzyme (CYP154H1QE), or 3 μM enzyme (CYP154F1QE and CYP154G1QE), 10 mM styrene and either 10 mM H_2O_2 (CYP154H1QE and CYP154G1QE reactions) or 5 mM H_2O_2 (CYP154F1QE reaction). The thioanisole oxidation reaction contained similar concentration of the respective CYPs, 1 mM thioanisole, and 1 mM H_2O_2

Thioanisole oxidation by peroxygenase enzymes is complicated by the non-enzymatic reaction of the substrates with H_2O_2 so less peroxide was used in these reactions (1 mM versus 10 mM). The sulfoxidation of thioanisole to methyl phenyl sulfoxide was catalysed by CYP154H1QE and CYP154G1QE (Figures 5B and S19). In addition to the main sulfoxide product, the enzymes also generated trace amounts of methyl phenyl sulfone, arising from further oxidation, totalling ~1% (Figure 5B, and Table S3) [40, 50, 81]. CYP154H1QE and CYP154G1QE catalysed the formation of 90 and 41 μM of methyl phenyl sulfoxide, per μM of enzyme, respectively (Table 2). Thioanisole oxidation reactions with WT CYP154H1 and

CYP154F1QE did not generate any products over the background levels generated in the no enzyme peroxide control reaction.



Scheme 2. Product distribution for the oxidation of styrene, ethylbenzene and thioanisole by the CYP154 enzymes. The product distribution of each is provided, CYP154H1QE (in blue), CYP154G1QE (in green) and CYP154F1QE (in red), The remainder of the oxidation products for styrene consisted of benzaldehyde (0.5%, 4% and 15%, respectively). The product distribution of the CYP154F1QE reactions was calculated from low product amounts.

The formation of styrene oxide, 1-phenylethanol and phenyl methyl sulfoxide can generate different enantiomeric forms, and we investigated the enantioselectivity of product formation using GC analysis. CYP154G1QE styrene and thioanisole bioconversion products indicated that the enzyme produces a 46% enantiomeric excess (e.e.) of (*R*)-styrene oxide and had a preference for the (*R*)-methyl phenyl sulfoxide enantiomer, with an enantiomeric excess of ~8% (Table 3). CYP154F1QE also showed a preference for (*R*)-styrene oxide with an enantiomeric excess of 22% (Table 3). CYP154H1QE favoured the formation of (*R*)-styrene oxide (enantiomeric excess of 60%) but favoured (*S*)-1-phenylethanol (85% enantiomeric excess). In the formation of the sulfoxide from thioanisole, CYP154H1QE preferred (*R*)-methyl phenyl sulfoxide with an enantiomeric excess of 46% (Table 3 and Figure S20).

Table 3. Enantioselectivity of the metabolites arising from the oxidation reactions of QE CYP154 enzymes from *T. fusca*. * Inversion of selectivity to favour the (*S*)-enantiomer.

450 Enzyme	((*R*)-Enantiomer (%)	(*S*(*S*)-Enantiomer (%) (	Enantiomeric excess) (%)
	(*R*)-1-styrene oxide	**(*S*)-1-styrene oxide)**	
CYP154H1QE1	80	20	60
WT CYP154H1	43	57	-13*
CYP154G1QE	73	27	46
CYP154F1QE	61	39	22
	(*R*)-1-phenyl methyl sulfoxide	**(*S*)-1-phenyl methyl sulfoxide**	
CYP154H1QE	73	27	46
WT CYP154H1	52	47	5
CYP154G1QE	54	46	8
	(*R*)-1-phenylethanol	**(*S*)-1-phenylethanol**	
CYP154H1QE1	7	92	85
WT CYP154H1	44	56	11

In comparison to the QE variant form, WT CYP154H1 favoured the formation of the alternate (*S*)-enantiomer of styrene oxide, with a lower enantioselectivity (Table 3). Similar enantioselectivity for the (*S*)-enantiomer was previously reported with WT CYP154H1 reactions via the monooxygenase pathway, supported by heterologous redox partners, Pdr and Pdx [50]. The altered selectivity observed in the oxidation of styrene by CYP154H1QE could be explained if the QE mutation results in an altered binding orientation of the substrate. Changes in CYP enzyme enantioselectivity resulting from mutations around the heme region has been observed previously in the epoxidation of styrene, while in other instances the stereoselectivity is maintained [81, 83].

The control of enzyme catalysed reactions to prevent or limit further oxidations is desirable to enhance regioselectivity and to improve yield, facilitate product recovery and purification as well as enabling greener biocatalytic processes. To investigate if H_2O_2 delivery could improve enzyme selectivity we varied the concentration and method of addition of H_2O_2 in the oxidation reactions. We chose CYP154H1QE ethylbenzene oxidation reactions for these assays as this

reaction showed the highest levels of product formation (Table 2). Reducing the H_2O_2 concentration from 10 to 2 mM decreased the extent of further oxidation by approximately two-fold, although at the expense of lower turnover numbers (Figure 6A). CYP154H1QE had TON values of 585 ± 130 with 10 mM H_2O_2 and 267 ± 18 with 2 mM H_2O_2.

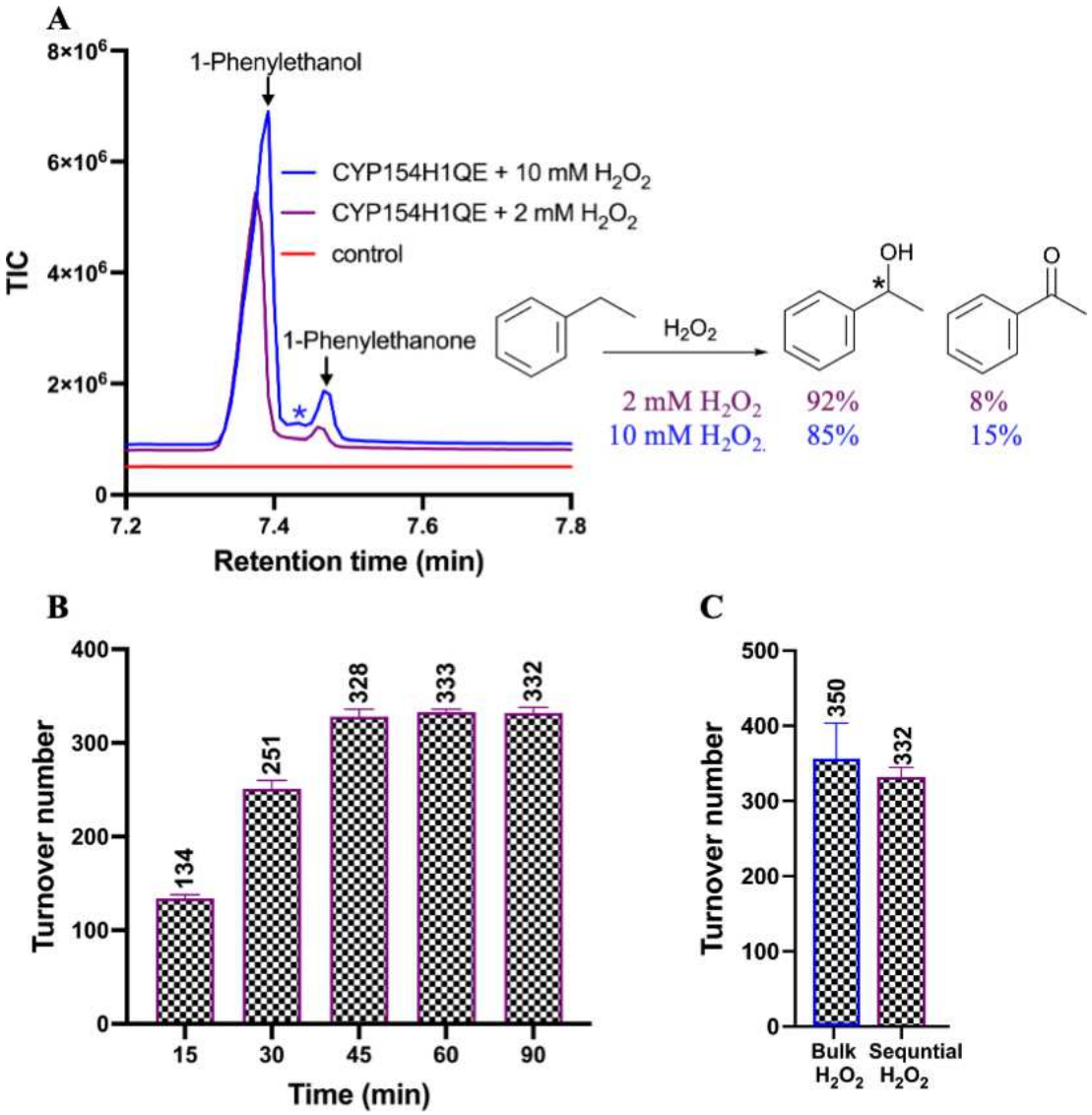


Fig. 6 The effect of concentration and mode of delivery of H_2O_2 on the selectivity of CYP154H1QE. (**A**) The reaction mixture contained 3 µM enzyme, 10 mM substrate and 10 or 2 mM H_2O_2. The control reaction contained no enzyme. (**B**) Reactions 2 µM enzyme, 10 mM ethylbenzene and 10 mM H_2O_2 added in 2 mM aliquots at 0, 15, 30, 45, and 60 min. (**C**) The reaction with a single (bulk) addition of 10 mM H_2O_2 is shown for comparison. TON is defined as the number of substrate oxidations per µM of CYP, calculated as the sum of generated 1-phenylethanol plus two equivalents of 1-phenylethanone. * Trace amounts of styrene oxide were generated with 10 mM H_2O_2 (< 1% of products)

To investigate if the method of delivery of the oxidant could improve selectivity without compromising TON, 10 mM H_2O_2 was supplied in bulk at the start of the reaction and by the sequential addition of five 2 mM aliquots at 0, 15, 30, 45, and 60 min (Figure 6B–C). For the sequential addition reaction, the TON of the enzyme was 134, 251 and 328, at 15, 30 and 45 min, respectively, after which, the TON was largely unchanged (Figure 6B). The proportion of 1-phenylethanone increased progressively over time, from 3-6% of the total products (Figure 6). When compared to the reaction with bulk addition of the oxidant the TON values were similar, but the sequential addition of H_2O_2 reduced the extent of further oxidation to the ketone relative to bulk addition (Figure 6B–C). In these reactions with 10 mM H_2O_2, trace amounts of styrene oxide were generated (< 1% of products) which could arise from desaturation of ethylbenzene to form styrene followed by epoxidation (Figure 6) [84, 85].

Experiments with 2 mM H_2O_2 were conducted to assess the formation of product over time and the efficacy of peroxide utilisation. Similar to the experiments above these showed a steady increase in product formation over the first 60-90 min of the reaction with a TON of 325 after 2 h (Figure S21). These experiments demonstrate that ~33% of the added peroxide was used to generate oxidised metabolites over 2 h. The monooxygenase activity of WT CYP154H1 (using 2 μM P450, 4 μM PdR, 20 μM Pdx) resulted in a product formation rate of 0.28 nmol min^{-1} $nmol^{-1}$ P450 with ethylbenzene and 6% coupling to NADH usage [50]. This compares to a rate of ~9 with the peroxygenase system (Figure 6 and Figure S21).

Oxidation reactions with other substrates

While the oxidation of the compounds tested above by CYP154H1QE was good for a new peroxygenase enzyme, we wished to further assess the substrate preference of the CYP154G1 and CYP154F1 enzymes. Given the potential differences in substrate specificities within the CYP154 family enzymes we tested these enzymes with progesterone, geraniol and the aromatic

compounds, indole and 1-methoxynaphthalene. Like CYP154H1QE, CYP154F1QE and CYP154G1QE did not generate detectable oxidative activity towards progesterone, (Figure S22). The lack of observed activity reflecting that progesterone also falls outside the substrate preference of CYP154G1 and CYP154F1.

In H_2O_2-driven geraniol oxidation reactions, CYP154F1QE catalysed the hydroxylation of the monoterpenoid to yield 8-hydroxygeraniol, the same metabolite that is reported for the wild-type enzyme [51]. However, under these conditions 3 µM enzyme and 500 µM substrate, the hydroxylated product was generated in low yield, ~6% substrate conversion, a TON of ~10 (Scheme 3 and Scheme S1 and Figure S23-S25). Reactions of CYP154G1QE with geraniol gave higher levels of product (~25% substrate conversion, a TON of ~41) but the reaction was unselective generating a mixture of metabolites. These were identified as arising from 25% geranial (G-CHO), 7% 2,3-epoxygeraniol (2,3-epoxy-G-OH), 20% 6,7-epoxygeraniol (6,7-epoxy-G-OH), 3% 8-oxogeraniol (8-O-G-OH) and the major product 45% 8-hydroxygeraniol (8-OH-G-OH) (Figure 7A, Scheme 3, Scheme S1 and Figure S23-S25) [86].

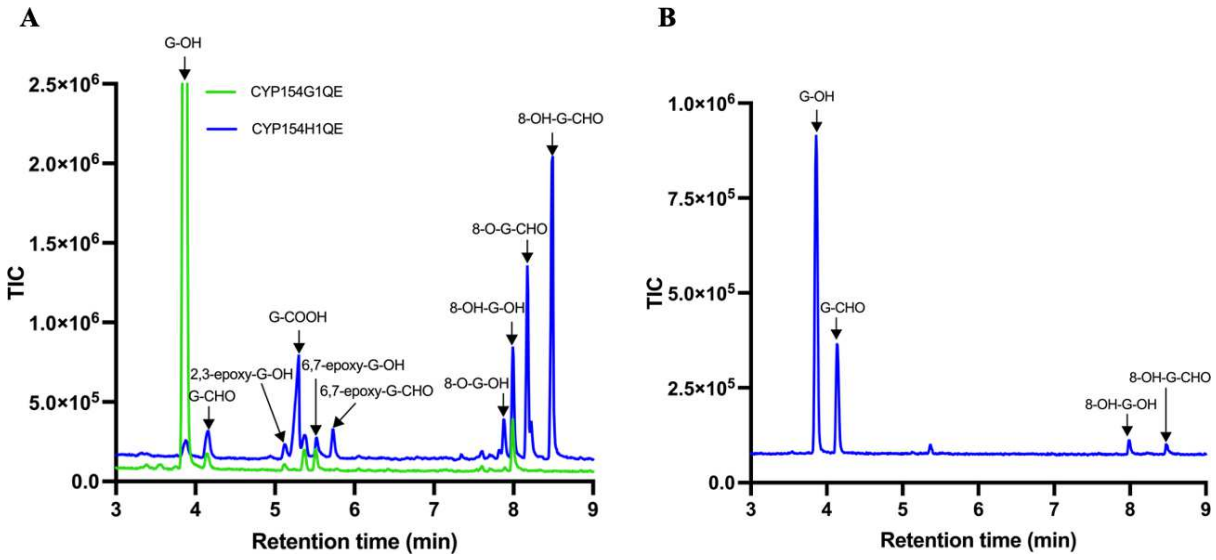
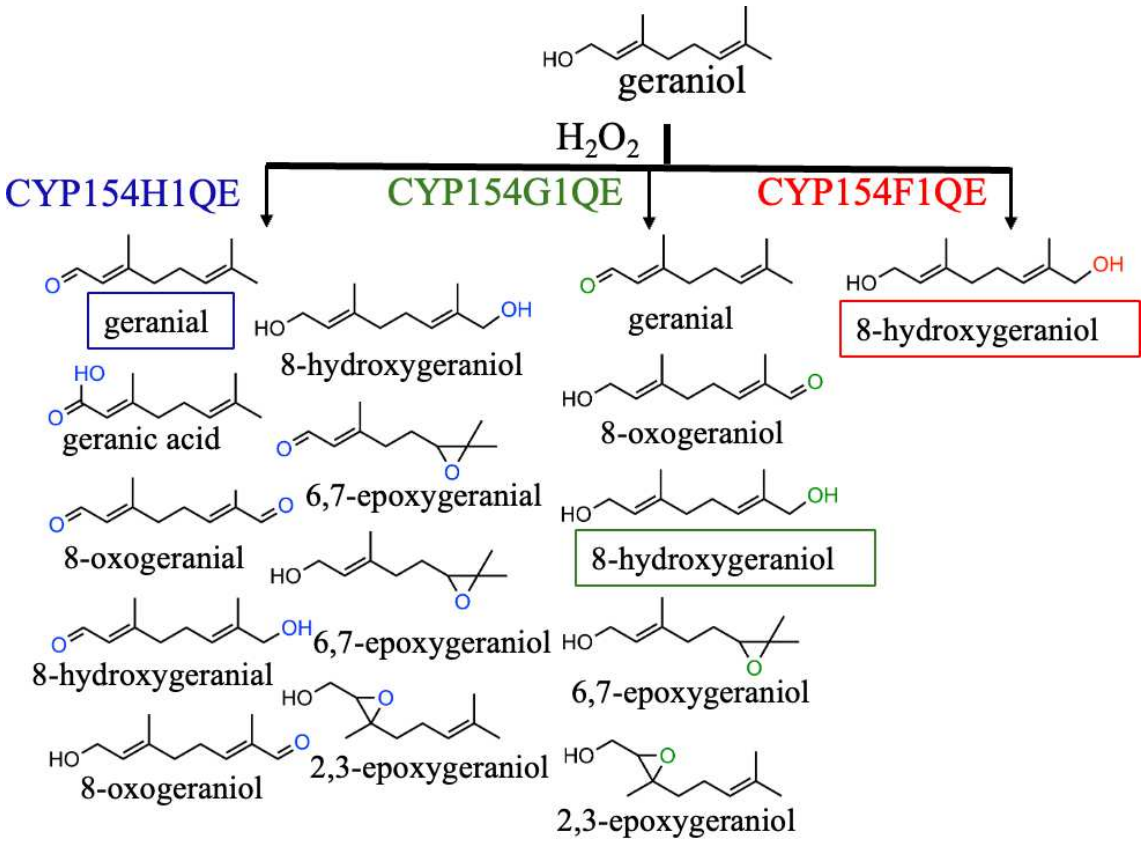


Fig. 7 Oxidation of geraniol by CYP154H1QE and CYP154G1QE. (**A**) The reaction mixture contained 3 µM enzyme in Tris HCl buffer pH 7.4, 500 µM geraniol and 10 mM H_2O_2 for 3 h, reactions contained 3 µM CYP154H1QE and CYP154G1QE. (**B**) This reaction contained a lower concentration (0.5 µM) of CYP154H1QE for 1 h (See Scheme 3 and Scheme S1 for full analysis)

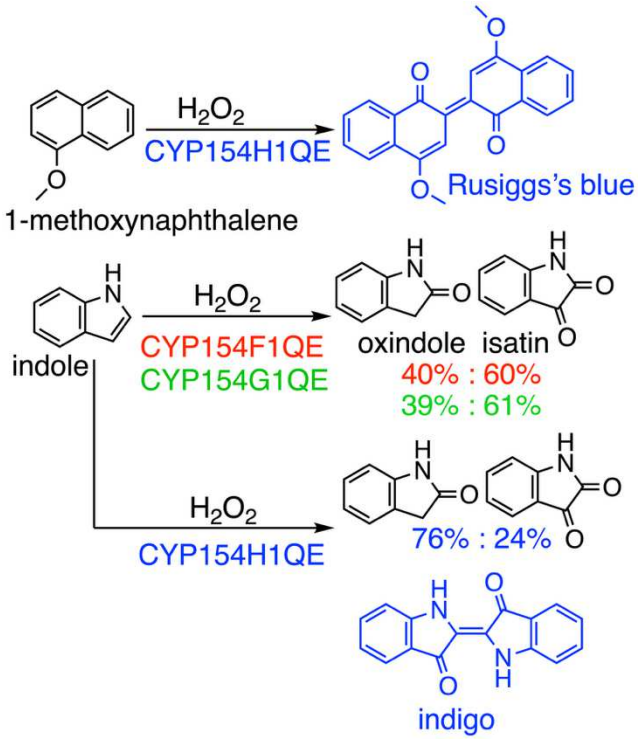


Scheme 3. The major oxidation metabolites form geraniol oxidation reactions by CYP154H1QE, CYP154G1QE and CYP154F1QE. The major products generated by each enzyme are highlighted in boxes. Products geraniol (G-OH), geranial (G-CHO), 2,3-epoxygeraniol (2,3-epoxy-G-OH), geranic acid (G-COOH), 6,7-epoxygeraniol (6,7-epoxy-G-OH), 6,7-epoxygeranial (6,7-epoxy-G-CHO), 8-oxogeraniol (8-O-G-OH), 8-hydroxygeraniol (8-OH-G-OH), 8-oxogeranial (8-O-G-CHO) and 8-hydroxygeranial (8-OH-G-CHO).

Under the same reaction conditions CYP154H1QE converted all of the geraniol to a complex mixture of metabolites. This includes geranial, geranic acid, several epoxides, and the 8-oxo and 8-hydroxy metabolites of geraniol and geranial (Figure 7, Scheme 3, Scheme S1, and Figures S23-S25) [86]. The sum of metabolites corresponded to an excess of 167 turnovers when the further oxidations are considered. Using a lower concentration of CYP154H1QE (0.5 μM), we observed a clear preference for the initial generation of the aldehyde, geranial, and its further oxidation to 8-hydroxygeranial, as well as the terminal hydroxylation of the parent terpenoid to 8-hydroxygeraniol. The oxidation at the substrate alcohol is consistent with the

binding data which suggested the alcohol moiety was positioned close to the heme (Figure 7B and Figure S9).

We next tested two aromatic compounds that have been shown to generate coloured metabolites. Colorimetric reactions are valued for their usefulness for assessing the product range and product formations levels and are suitable for high throughput screening processes. The oxidation of indole to indigo or indirubin by CYP154H1 (wild type) has been previously reported and other enzymes [50, 87]. Similarly, the formation of the coloured Russig's blue from oxidation of 1-methoxynaphthalene by the peroxygenase CYP152A1 enzyme and CYP102 enzyme has also been reported [72, 88]. We therefore investigated the oxidation of indole and 1-methoxynaphthalene by the mutant CYP154 enzymes (Scheme 4).



Scheme 4. Oxidation of indole and 1-methoxynaphthalene by CYP154H1QE, CYP154G1QE and CYP154F1QE enzymes from *T. fusca.* The coloured compounds formed by CYP154H1QE catalysed oxidation reactions are presented in blue.

CYP154F1QE and CYP154G1QE did not convert 1-methoxynaphthalene into a coloured metabolite. The reactions with CYP154H1QE did turn blue, generating 57 ± 1 μM (per μM of

enzyme), of 4,4-Russig's blue. HPLC and GC-MS analysis showed the formation of other product metabolites, (Figures S26A-B, S27-S28) including a hydroxylated metabolite and one resulting from oxidative demethylation (1,4-naphthalenedione) (Figure S28).

All three mutant CYPs were able to oxidise indole, HPLC analysis showed a mixture of oxindole and isatin were the major products with several other minor products being formed (Figure 8 and Table S4). GCMS analysis showed that CYP154G1QE, in addition to oxindole (2-oxoindole) and isatin generated a metabolite with an MS consistent with *N*-(2-formylphenyl)formamide which would result from the oxidative cleavage of the indole pyrrole ring (Figure S29). CYP154G1QE, CYP154F1QE and CYP154H1QE generated 16 ± 6 μM, 17 ± 3 μM, and 381 ± 90 μM of oxindole per μM of enzyme, respectively (Table S4). Isatin was generated in amounts of 24 ± 7 μM, 25 ± 5 μM and 121 ± 10 μM per μM of CYP154G1QE, CYP154F1QE and CYP154H1QE, respectively (Table S4). CYP154H1QE generated the most product and experiments using 0.5 μM and 1 mM indole enabled the calculation of TON of 1300 ± 20 (Figure S30A). In addition to generating the most product, CYP154H1QE was the only enzyme that resulted in a detectable blue coloured indigo compound (Figure 8A-B, Figures S27, S30A-B and Table S4). Control reactions of CYP154H1QE with 2-oxoindole and isatin did not generate indigo and demonstrated that isatin was not derived from 2-oxindole (Figure S31). Isatin and indigo could potentially be generated from undetected 3-oxindole [89, 90]. Control reactions with 2-oxindole and isatin in the absence of enzyme highlighted that some of the other minor products in the indole reactions could be generated from their reaction with H_2O_2 (Figure S31).

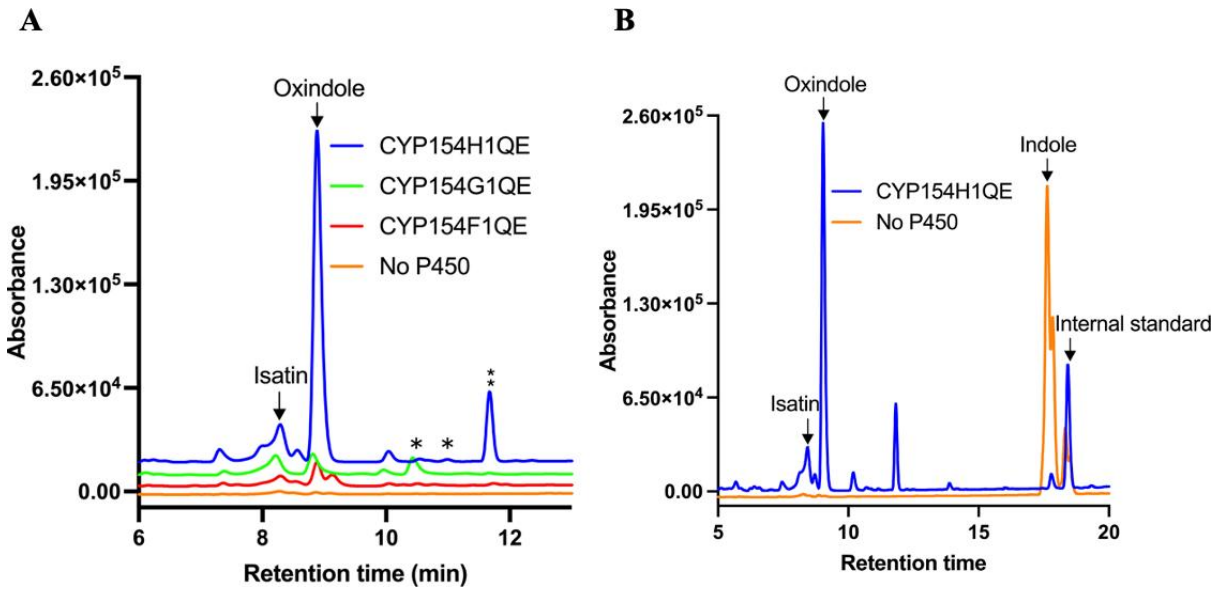


Fig. 8 HPLC analysis of indole oxidation catalysed by CYP154H1QE, CYP154G1QE and CYP154F1QE. The reaction mixtures contained (**A**) 1 μM enzyme or (**B**) 2 μM enzyme, 1 mM indole and 10 mM H_2O_2 (CYP154H1QE and CYP154G1QE reactions) or 5 mM H_2O_2 (CYP154F1QE reaction) for 24 h. ∗, isatin further oxidation metabolite. ⁑, H_2O_2 oxidation of 2-oxindole (oxindole; see Figure S30A-B)

We also generated the CYP154F1 WT enzyme to test its activity compared to the QE variant in case the mutations we had introduced had a negative effect on the peroxygenase activity for this CYP154 enzyme given the low levels of product generated. The WT enzyme was produced in good yield, and some binding of geraniol was detected by UV-Vis absorbance spectroscopy (Figure S32). However, the peroxide driven oxidation reactions of the WT enzyme with substrates, which were oxidised by the QE variant, generated lower levels of the metabolites (Figure S33). This agrees with the observation that the QE variant improves the peroxygenase activity with the CYP154 enzymes as observed with CYP154H1 and CYP154C35.

The formation of coloured products (e.g. Russig's blue and indigo) from 1-methoxynaphthalene and indole could be useful in screening of related compounds with CYP154H1 or in the optimisation of its peroxygenase activity using directed evolution or high-throughput protein engineering method (Figure S27) [87, 91-93].

Reactions with labelled H_2O_2 and ascorbic acid

To gain insight into the catalytic mechanisms of these enzyme biotransformations, we carried out reactions with ^{18}O labelled H_2O_2. Experiments with isotopically labelled $H_2{}^{18}O_2$ and CYP154H1QE with styrene, ethylbenzene and thioanisole all confirmed that the oxygen incorporated into the formed metabolites is sourced from the H_2O_2 (Figure S34-S40). With 1-methoxynaphthalene, two of the three observable GCMS products incorporated ^{18}O from enzyme supported catalysis. However, the 1,4-naphthalenedione, which was formed only in the reactions of CYP154H1QE with 1-methoxynaththalene did not. We conclude that in the enzyme-catalysed reaction O-demethylation was followed by air autoxidation (Figure S37) [94].

CYP154F1QE, CYP154G1QE and CYP154H1QE indole oxidation reactions supported by ^{18}O labelled H_2O_2, indicated that the ^{18}O-atom was incorporated into the 2-oxindole major product (Figure S39). Interestingly, the *N*-(2-formylphenyl)formamide formed in CYP154G1QE rection with indole did not have the ^{18}O incorporated (Figure S40). Control reactions without enzyme and H_2O_2 or with the enzyme but without H_2O_2 did not yield any product. The *N*-(2-formylphenyl)formamide could be formed by oxidative cleavage of the pyrrole ring through a dioxygenase like function that is activated by H_2O_2. This type of dioxygenase activity towards indole in the presence of H_2O_2 has been previously reported for the dehaloperoxidase-hemoglobin from *Amphitrite ornata* [95].

Oxidation reactions were carried out in the presence of ascorbic acid to determine the effect of this free radical and reactive oxygen species scavenger on product formation (Figure 9). In the presence of ascorbic acid, the level of product formation was similar with geraniol and 1-methoxynaphthalene 98% and 90%, respectively.

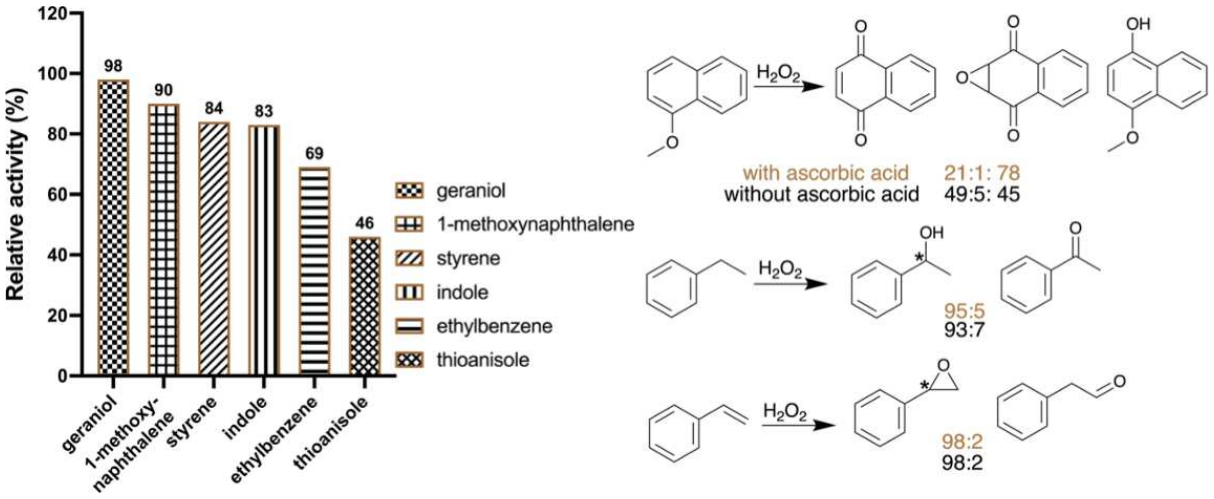


Fig. 9 Effect of ascorbic acid on the activity of CYP154H1QE. The relative enzyme activity was measured using product formation or substrate utilisation (1-methoxynaphthalene). The enzyme activity in the absence of ascorbic acid as 100%. Indole and geraniol reactions generated oxindole and geranial in presence or absence of ascorbic acid. The reaction mixture contained 3 μM of enzyme in Tris-HCl buffer pH 7.4, 2 mM H_2O_2 and 10 mM substrate (styrene and ethylbenzene). Reactions with thioanisole contained 3 μM of enzyme, 1 mM substrate and 1 mM H_2O_2. Reactions with indole and geraniol contained 1 μM enzyme in Tris-HCl buffer pH 7.4, 2 mM H_2O_2 and 1 mM substrate (indole) or 0.5 mM geraniol. Reactions with 1-methoxynaphthalene contained 2 μM enzyme in Tris-HCl buffer pH 7.4, 2 mM H_2O_2 and 1 mM substrate. Control reactions were carried out in identical conditions without the addition of ascorbic acid

Thioanisole sulfoxidation by CYP154H1QE in the presence of ascorbic acid was reduced to 46% (Figure 9). This could potentially be related to the lower levels of H_2O_2 in this reaction mixture when compared to other substrates as ascorbic acid can act as a reductant of H_2O_2 which directly oxidised the thioanisole and compete with the peroxide driven enzymatic oxidation (1 mM versus 10 mM peroxide is used in these reactions) (Figure 9) [96]. The product distribution from ethylbenzene oxidation in the presence of ascorbic acid was only slightly modified with a slight lowering of the amount of the ketone overoxidation metabolite, 1-phenylethanone (Figure 9). With 1-methoxynaphthalene, the formation of the hydroxylated metabolite was more favoured over the other metabolites in the presence of ascorbic acid. In the oxidation of geraniol, styrene and thioanisole, there were no significant difference in the product distribution.

Thermostability of the enzymes

Protein thermostability is a property that is desirable for many biotechnological applications for enhanced biocatalytic lifespan as well as the ease of transportation and storage [29, 71, 97]. As *T. fusca* XY is a moderately thermophilic bacterium and the WT CYP154H1 has been reported to be stable to heating at 50 °C, maintaining 90% residual activity, we assessed the temperature tolerance of the three engineered enzymes [50]. We heated the enzymes for 1 h at temperatures ranging from 45-80 °C and determined the residual enzyme activity by measuring product formation in the styrene epoxidation reaction (Figure 10). The $^{60}T_m$ of CYP154G1QE, CYP154H1QE and CYP154F1QE was 60 °C, 61 °C and 72 °C, respectively (Figure 10). The $^{60}T_m$ of CYP154C35QE from *Nocardia otitidiscaviarum* was 42.8 °C, which is significantly lower than these CYP154 enzymes from the H, G and F subfamilies from *T. fusca* [36].

After heating at 50 °C for 1 h, CYP154G1QE, CYP154H1QE and CYP154F1QE retained residual activities of 84%, 95% and 94%, respectively. On heating for 1 h at 60 °C, the residual activities were 40%, 61% and 75% for CYP154G1QE, CYP154H1QE and CYP154F1QE, respectively. Incubation for 1 h at 65 °C completely inactivated CYP154H1QE and CYP154G1QE, however, CYP154F1QE was still active with a residual activity of 61%. CYP154F1QE retained 17% activity at 80 °C, making it the most stable CYP isoform of the three enzymes tested in the current study (albeit with the lowest activity, making assessment of its thermostability more challenging). An important observation is that the introduction of the mutations to CYP154H1QE to engender peroxygenase function did not significantly reduce its thermostability when compared to that reported for the WT CYP154H1.

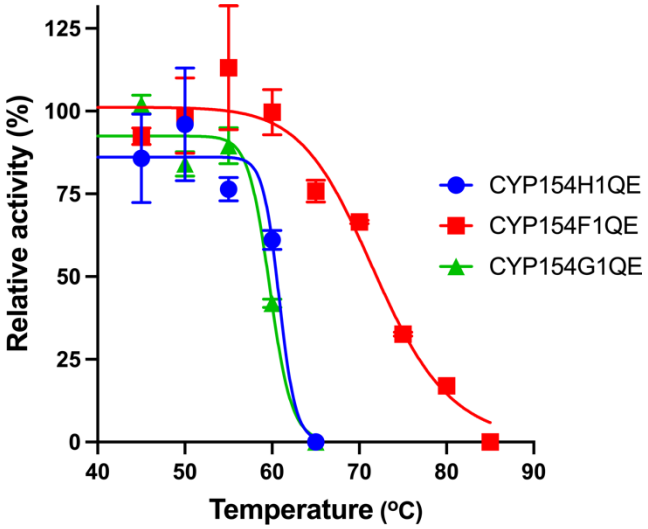


Fig. 10 Temperature stability of CYP154H1QE, CYP154G1QE and CYP154F1QE. The relative enzyme activity was measured using the quantity of styrene oxide formed after 1 h incubation at each temperature. The amount of styrene oxide formed by the unincubated enzyme as 100%. The data was fitted into a Hill-type equation, and the line of best-fit with corresponding $^{60}T_m$ were extracted. We note that the CYP154F1QE data is obtained with lower levels of product formation

By way of comparison, bacterial CYP107PQ1 from *Meiothermus ruber*, is stable at 60 ℃ for 1 h with no loss of activity [29]. CYP119A1 from *Sulfolobus acidocaldarius*, is reported to be stable at 80 ℃, it has a melting temperature of 91 ℃ [56, 98, 99]. CYP175A1 from the thermophilic bacterium *Thermus thermophilus*, is observed to have a melting temperature of 88 ℃ [100, 101]. While the CYP154 enzymes in this study may not be as robust as some of these enzymes, they are significantly higher in comparison to CYP154C8 and CYP154C35, which completely denatured between 40 and 50 °C, and other bacterial mesophilic CYPs [54, 59]. The thermostability of these CYP154 enzymes are similar to that of CYP107PQ1 which could be stored at 30 °C for more than 1 year.

Comparison of CYP154 structural models

To interrogate the observed differences in substrate preference and activity of the CYP154 enzymes, we compared the sequences and generated structural models of the QE variants of

the three CYP154 enzymes using AlphaFold 3 (Figure S41-S43) [102]. For validation, the sequence and structural models were aligned with the available X-ray crystal structure of that of a close relative from within the same family, CYP154C5 with progesterone bound (PDB entry 4J6C). The aligned structures had RMSD values of 1.076, 1.175 and 1.052, respectively. These models feature the overall conserved CYP characteristic fold with a central heme core and the canonical A/G-G-X-D/E-T-T/S oxygen bonding groove within the I-helix (Figure S42). Some differences were observed in the sequence close to the oxygen-binding (O_2-binding) groove, CYP154F1QE and CYP154G1QE have a phenylalanine, F237 and F235, respectively, in the variable amino acid position (X). This residue is replaced with a histidine in CYP154H1QE and CYP154C5 (Figure S42D).

The residues that constitute the active sites of the three enzymes were compared to those of CYP154C5 and other CYP154C subfamily enzymes (Figure 11 and Table S6). While all these enzymes belong to the same CYP family they have low overall sequence homology to members of different subfamilies (as low as 34.2 %, Table S7). This highlights the sequence diversity among the chosen enzymes, especially among the H1, G1 and F1 members from *T. fusca*. Despite this overall low sequence identity, there were relatively few changes in the amino acids that constitute the active site. However, despite the small number of changes the enzymes have divergent substrate ranges (Figure 11). Potentially important differences were observed at P289 of CYP154H1 which is conserved in CYP154C5 but is a serine in CYP154G1 and CYP154F1. I157 of CYP154H1 was conserved in CYP154C5 and CYP154G1 but not CYP154F1 where it was replaced by a phenylalanine. L93 of CYP154H1 was conserved in CYP154G1 and CYP154F1 but was replaced with a phenylamine in CYP154C5. I239 of CYP154H1 was a leucine in CYP154G1 and CYP154F1 and alanine in CYP154C5. F293 was unique to CYP154H1 and aligned with a leucine the other three CYP154 enzymes.

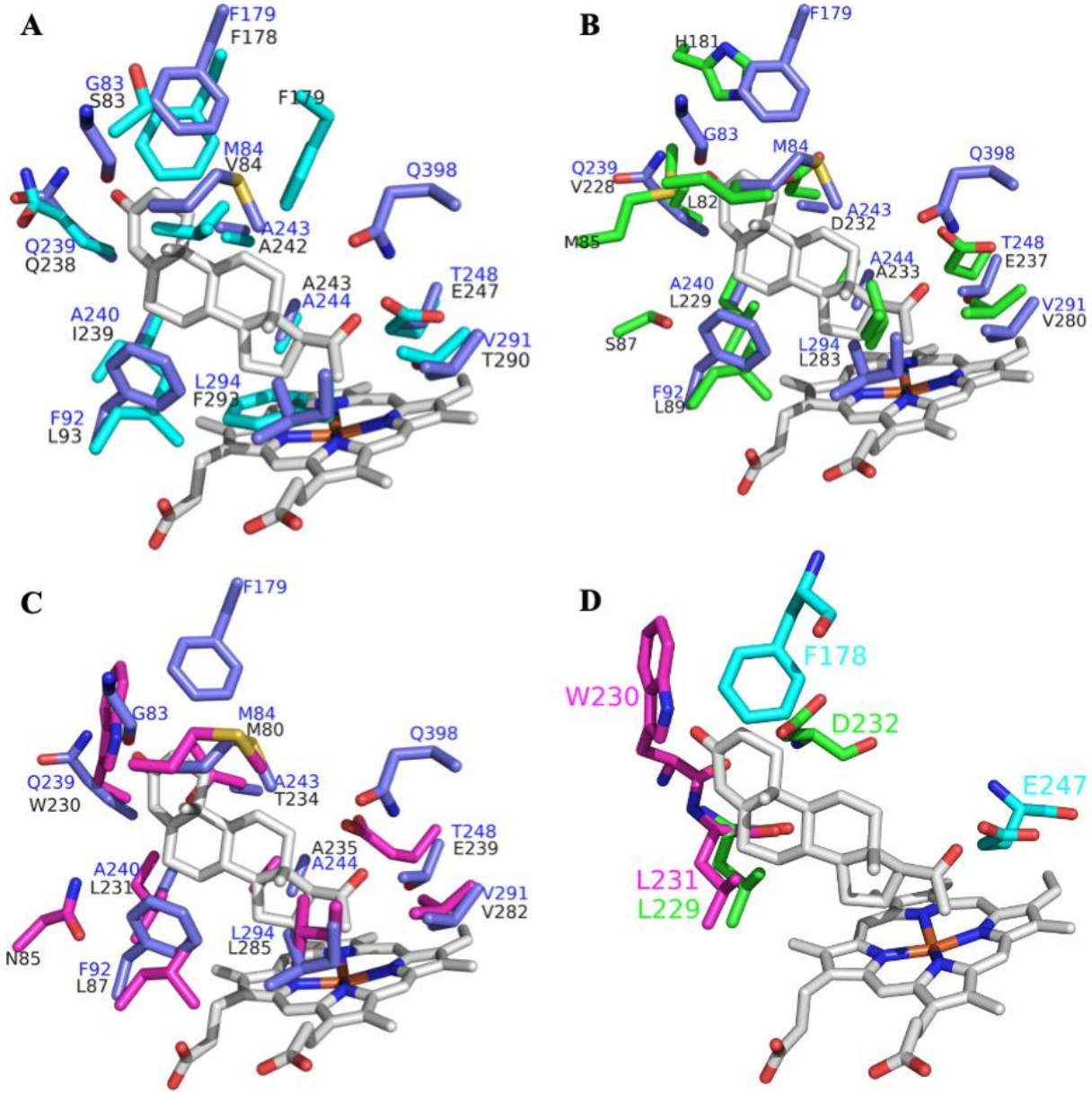


Fig. 11 Overlay of the active site residues of CYP154H1QE, CYP154G1QE and CYP154F1QE derived from AlphaFold models with those of the X-ray crystal structure of CYP154C5 (PDB entry 4J6C). **A.** CYP154H1QE (cyan), **B.** CYP154G1QE (green) and **C.** CYP154F1QE (pink). The CYP154C5 enzyme residues are depicted in blue. **D.** The residues within 2 Å of progesterone in the CYP154 models. Residues are shown relative to progesterone bound in CYP154C5. Residues in CYP154G1QE, CYP154F1QE and CYP154H1QE are labelled in green, magenta and cyan, respectively

In the models, we observed potential steric clashes of residues with progesterone if this substrate binds as it does in CYP154C5 (Figure 11D). This agrees with the observation that progesterone is not a substrate for any of these CYP154 enzymes. The determination of X-ray

crystal structures with substrate bound and further protein engineering experiments would better ascertain the importance of these residues. This would also generate more reliable data for molecular dynamic simulations to better determine the substrate range and mechanism of the enzymes which will facilitate the design of better biocatalysts.

Conclusions

In conclusion, we engineered peroxygenase function into three enzymes from *T. fusca* and demonstrated that different subfamilies within the CYP154 exhibit difference in substrate scope and product selectivity. We assessed the peroxygenase function of three enzymes from *T. fusca* belonging to the H, F and G subfamilies of the CYP154 family, and demonstrated that each had its own distinct substrate range which was different to that of other CYP154 enzymes including the CYP154C subfamily members. These enzymes performed the H_2O_2 supported oxidation of a range of substrates with catalytic activity increase in the order CYP154F1QE < CYP154G1QE < CYP154H1QE. The lower catalytic activity of CYP154F1QE likely reflects that its physiological substrate is yet to be identified. The activity of the CYP154H1QE mutant was significantly higher than the nugatory levels obtained with the WT enzyme in agreement with the CYP154C35 enzymes demonstrating the importance of the mutations we used.

The oxidation products we have generated with the QE enzymes from *T. fusca* are chemically relevant building blocks in the synthesis of fine chemicals [14, 103-109]. The biocatalytic synthesis of oxindoles is relevant in medicinal chemistry, due to the biological and synthetic potentials of oxindole derivatives [14, 106]. The reactions with CYP154G1 showed a dioxygenase-like indole cleavage activity which would be worthy of further investigation. The observation of geraniol oxidation at different sites could lead to systems for the oxidation of linear monoterpenoids at selected positions. The activities of the CYP154 peroxygenase enzymes reported here (500-1300 TON for good substrate/enzyme combinations, and in excess of 5000 for CYP154C35 with an optimal substrate) are promising when compared to other peroxygenase enzymes. Heme peroxygenase enzymes including CYP152s and UPOs have undergone extensive optimisation processes over a long period of time which has enabled increased turnover numbers by one to two orders of magnitude or even higher. The activity we report here is adequate to establish the likely function (or lack of) of each CYP154 enzyme. It

provides a useful starting point for optimisation for larger scale production processes and optimisation studies.

The enzymes showed various degrees of enantioselectivity in certain reactions, with up to ~80% ee for the formation of (*S*)-1-phenylethanol. This is a significant increase compared to the WT enzyme a could be improved with protein engineering efforts. The selectivity of the CYP154H1QE enzyme for the alcohol metabolite over the ketone product could be modulated by the concentration and mode of addition of the H_2O_2.

CYP154H1QE, CYP154G1QE and CYP154F1QE were moderately thermostable with melting temperatures between 60-71 ℃. This would remove the need for cryostorage and could extend catalyst lifetime. They were produced in a soluble form in high yield using standard media and *E. coli* strains in shake flasks without the need for optimisation or expensive additives such as aminolevulinic acid. These factors when coupled with the removal of the requirement for additional protein partners and expensive nicotinamide cofactors offers some advantages and over UPOs and CYP monooxygenases as well as offering opportunities for complementary activities on a wider range of substrates. Therefore, these enzymes are promising platforms for engineering robust peroxygenase biocatalysts for environmentally friendly synthesis of chiral building blocks, as well as oxidised metabolites of linear terpenoids and indoles. Future work will involve identifying additional substrates for these enzymes, in particular for CYP154F1 which had low activity for all of those that were tested. More efficient peroxygenase variants of CYP154H1, CYP154G1 and CYP154F1 could be developed along with enhanced peroxide delivery methods to fully harness the biocatalytic potential of these enzymes. The work undertaken here identifying colorimetric assays for the higher throughput assessment of enzyme activity will facilitate that process.

Statements and Declarations

Acknowledgements

This work was funded, in part, through Australian Research Council Grant DP240101500 (to S.G.B. and others). O.O. was supported by University of Adelaide International Scholarships.

Competing Interests

S.G.B. is an inventor on a patent related to this work (PCT/AU2024/050934 and WO2025/043300).

Data Availability Statement

All data generated or analysed during this study are included in this published article and its supplementary information files.

References

1. Yan Y, Wu J, Hu G, Gao C, Guo L, Chen X, Liu L, Song W (2022) Current state and future perspectives of cytochrome P450 enzymes for C–H and C=C oxygenation. Synthetic and Systems Biotechnology 7:887-99. https://doi.org/10.1016/j.synbio.2022.04.009

2. Alves Chagas BC, Jia H, Brixius B, Brixius-Anderko S (2025) The curious family of cytochrome P450 4F fatty acid ω-hydroxylases: recent developments in their function and relevance for human health. Open Biology 15:https://doi.org/10.1098/rsob.250115

3. Zhao S, Liu Y (2025) Mechanistic investigation on the C–C bond cleavage of α-hydroxy ketone catalyzed by engineering P450 monooxygenase enzyme F182L-CYP199A4. Inorganic Chemistry 64:11342-56. https://doi.org/10.1021/acs.inorgchem.4c05390

4. Greule A, Stok JE, De Voss JJ, Cryle MJ (2018) Unrivalled diversity: the many roles and reactions of bacterial cytochromes P450 in secondary metabolism. Natural Product Reports 35:757-91. https://doi.org/10.1039/c7np00063d

5. Guengerich FP (2002) Cytochrome P450 enzymes in the generation of commercial products. Nature Reviews 1:359-66. https://doi.org/10.1038/nrd792

6. Shoji O, Watanabe Y (2014) Peroxygenase reactions catalyzed by cytochromes P450. Journal of Biological Inorganic Chemistry 19:529-39. https://doi.org/10.1007/s00775-014-1106-9

7. Podgorski MN, Akter J, Churchman LR, Bruning JB, De Voss JJ, Bell SG (2024) Engineering peroxygenase activity into cytochrome P450 monooxygenases through modification of the oxygen binding region. ACS Catalysis 14:7426-43. https://doi.org/10.1021/acscatal.4c01326

8. Milhim M, Hartz P, Gerber A, Bernhardt R (2019) A novel short chain dehydrogenase from *Bacillus megaterium* for the conversion of the sesquiterpene nootkatol to (+)-nootkatone. Journal of Biotechnology 301:52-5. https://doi.org/10.1016/j.jbiotec.2019.05.017

9. Girhard M, Machida K, Itoh M, Schmid RD, Arisawa A, Urlacher VB (2009) Regioselective biooxidation of (+)-valencene by recombinant *E. coli* expressing CYP109B1 from *Bacillus subtilis* in a two-liquid-phase system. Microbial Cell Factories 8:36. https://doi.org/10.1186/1475-2859-8-36

10. Sowden RJ, Yasmin S, Rees NH, Bell SG, Wong L-L (2005) Biotransformation of the sesquiterpene (+)-valencene by cytochrome P450cam and P450BM-3. Organic & Biomolecular Chemistry 3:57. https://doi.org/10.1039/b413068e

11. Fu N, Yang Z-L, Pauchet Y, Paetz C, Brandt W, Boland W, Burse A (2019) A cytochrome P450 from the mustard leaf beetles hydroxylates geraniol, a key step in

iridoid biosynthesis. Insect Biochemistry and Molecular Biology 113:103212. https://doi.org/https://doi.org/10.1016/j.ibmb.2019.103212

12. Sonomoto K, Hoq MM, Tanaka A, Fukui S (1983) 11β-hydroxylation of cortexolone (Reichstein Compound S) to hydrocortisone by *Curvularia lunata* entrapped in photo-cross-linked resin gels. Applied and Environmental Microbiology 45:436-43. https://doi.org/doi:10.1128/aem.45.2.436-443.1983

13. Hosobuchi M, Kurosawa K, Yoshikawa H (1993) Application of computer to monitoring and control of fermentation process: microbial conversion of ML-236B Na to pravastatin. Biotechnology and Bioengineering 42:815-20. https://doi.org/https://doi.org/10.1002/bit.260420705

14. Wang HH, Miao RP, Wang YF, Wan NW (2025) Biocatalytic approaches for the synthesis of oxindoles. ChemCatChem https://doi.org/10.1002/cctc.202500591

15. Li F, Shen C, He Y, Lu H, Gu R, Yao J, Zhang Z, Mei F, Zhao T, Guo X, Xue N, Ding W (2025) Proper aggregation of Pt is beneficial for the epoxidation of styrene by O2 over Ptx/γ-Al2O3 catalysts. Nanoscale 17:7474-81. https://doi.org/10.1039/d4nr05256k

16. Sharma AS, Sharma VS, Kaur H, Varma RS (2020) Supported heterogeneous nanocatalysts in sustainable, selective and eco-friendly epoxidation of olefins. Green Chemistry 22:5902-36. https://doi.org/10.1039/d0gc01927e

17. Rabe KS, Kiko K, Niemeyer CM (2008) Characterization of the peroxidase activity of CYP119, a thermostable P450 from *Sulfolobus acidocaldarius*. ChemBioChem 9:420-5. https://doi.org/10.1002/cbic.200700450

18. Lee JHZ, Podgorski MN, Moir M, Gee AR, Bell SG (2022) Selective oxidations using a cytochrome P450 enzyme variant driven with surrogate oxygen donors and light. Chemistry – A European Journal 28:e202201366. https://doi.org/https://doi.org/10.1002/chem.202201366

19. O'Reilly E, Köhler V, Flitsch SL, Turner NJ (2011) Cytochromes P450 as useful biocatalysts: addressing the limitations. Chemical Communications 47:2490-501. https://doi.org/10.1039/c0cc03165h

20. Bernhardt R, Urlacher VB (2014) Cytochromes P450 as promising catalysts for biotechnological application: chances and limitations. Applied Microbiology and Biotechnology 98:6185-203. https://doi.org/10.1007/s00253-014-5767-7

21. Wang Y, Pan H, Wang F, Shen C (2024) Microbial P450 repertoire (P450ome) and its application feasibility in pharmaceutical industry, chemical industry, and environmental protection. Biotechnology and Bioengineering 121:7-25. https://doi.org/https://doi.org/10.1002/bit.28565

22. Zhao P, Kong F, Jiang Y, Qin X, Tian X, Cong Z (2023) Enabling peroxygenase activity in cytochrome P450 monooxygenases by engineering hydrogen peroxide

tunnels. Journal of the American Chemical Society 145:5506-11. https://doi.org/10.1021/jacs.3c00195

23. Ma N, Chen Z, Chen J, Chen J, Wang C, Zhou H, Yao L, Shoji O, Watanabe Y, Cong Z (2018) Dual-functional small molecules for generating an efficient cytochrome P450BM3 peroxygenase. Angewandte Chemie International Edition 57:7628-33. https://doi.org/10.1002/anie.201801592

24. Tang T, Wang R, Chen Y (2026) Engineering a cytochrome P450 enzyme as a peroxygenase for selective hydroxylation of steroids. Nature Communications 17:1996. https://doi.org/10.1038/s41467-026-69211-8

25. Aschenbrenner JC, Ebrecht AC, Smit MS, Opperman DJ (2024) Revisiting strategies and their combinatorial effect for introducing peroxygenase activity in CYP102A1 (P450BM3). Molecular Catalysis 557:113953. https://doi.org/https://doi.org/10.1016/j.mcat.2024.113953

26. Cirino PC, Arnold FH (2003) A self-sufficient peroxide-driven hydroxylation biocatalyst. Angewandte Chemie International Edition 42:3299-301. https://doi.org/https://doi.org/10.1002/anie.200351434

27. Fan S, Cong Z (2024) Emerging strategies for modifying cytochrome P450 monooxygenases into peroxizymes. Accounts of Chemical Research 57:613-24. https://doi.org/10.1021/acs.accounts.3c00746

28. Podgorski MN, Harbort JS, Lee JHZ, Nguyen GTH, Bruning JB, Donald WA, Bernhardt PV, Harmer JR, Bell SG (2022) An altered heme environment in an engineered cytochrome P450 enzyme enables the switch from monooxygenase to peroxygenase activity. ACS Catalysis 12:1614-25. https://doi.org/10.1021/acscatal.1c05877

29. Das T, Hayball EF, Harlington AC, Bell SG (2025) A thermostable heme protein fold adapted for stereoselective C−H bond hydroxylation using peroxygenase activity. ChemBioChem 26:e202400737. https://doi.org/https://doi.org/10.1002/cbic.202400737

30. Shoji O, Fujishiro T, Nishio K, Kano Y, Kimoto H, Chien S-C, Onoda H, Muramatsu A, Tanaka S, Hori A, Sugimoto H, Shiro Y, Watanabe Y (2016) A substrate-binding-state mimic of H_2O_2-dependentcytochrome P450 produced by one-pointmutagenesis and peroxygenation of non-nativesubstrates. Catalysis Science & Technology 6:5806-11. https://doi.org/10.1039/c6cy00630b

31. Nagano S, Poulos TL (2005) Crystallographic study on the dioxygen complex of wild-type and mutant cytochrome P450cam. Journal of Biological Chemistry 280:31659-63. https://doi.org/10.1074/jbc.m505261200

32. Harlington AC, Shearwin KE, Bell SG, Whelan F (2022) Efficient O-demethylation of ligninmonoaromatics using the peroxygenase activityof cytochrome P450 enzymes. Chemical Communications 58:13321-4. https://doi.org/10.1039/d2cc04698a

33. Harlington AC, Das T, Shearwin KE, Bell SG, Whelan F (2025) Structural insights into S-lignin O-demethylation via a rare class of heme peroxygenase enzymes. Nature Communications 16:1815. https://doi.org/10.1038/s41467-025-57129-6

34. Mallinson SJB, Machovina MM, Silveira RL, Garcia-Borràs M, Gallup N, Johnson CW, Allen MD, Skaf MS, Crowley MF, Neidle EL, Houk KN, Beckham GT, DuBois JL, McGeehan JE (2018) A promiscuous cytochrome P450 aromatic O-demethylase for lignin bioconversion. Nature Communications 9:2487. https://doi.org/10.1038/s41467-018-04878-2

35. Wolf ME, Hinchen DJ, McGeehan JE, Eltis LD (2024) Characterization of a cytochrome P450 that catalyzes the O-demethylation of lignin-derived benzoates. Journal of Biological Chemistry 300:107809. https://doi.org/10.1016/j.jbc.2024.107809

36. Osiebe O, Hayball EF, Yevstigneyev N, Abbott AM, Bell SG (2026) Scalable and stereoselective C–H bond hydroxylation of steroids using a designer heme-thiolate peroxygenase biocatalyst. The Journal of Organic Chemistry 91:1165-76. https://doi.org/10.1021/acs.joc.5c02818

37. Das T, Doyle ML, Hutchinson S, Bell SG (2026) Efficient isoprenoid oxidation by an engineered heme peroxygenase from the magnetotactic bacterium *Magnetospirillum gryphiswaldense*. Molecular Catalysis 593:115786. https://doi.org/https://doi.org/10.1016/j.mcat.2026.115786

38. Nelson DR (2009) The cytochrome P450 homepage. Human Genomics 4:59-65. https://doi.org/10.1186/1479-7364-4-1-59

39. Gront D, Syed K, Nelson DR (2025) Exploring P450 superfamily diversity with P450Atlas - online tool for automated subfamily assignment. Protein Science 34:e70057. https://doi.org/https://doi.org/10.1002/pro.70057

40. Von Bühler C, Le-Huu P, Urlacher VB (2013) Cluster screening: an effective approach for probing the substrate space of uncharacterized cytochrome P450s. ChemBioChem 14:2189-98. https://doi.org/10.1002/cbic.201300271

41. Winkelman DC, Nikolau BJ (2022) The Effects of Carbon source and growth temperature on the fatty acid profiles of *Thermobifida fusca*. Frontiers in Molecular Biosciences 9:https://doi.org/10.3389/fmolb.2022.896226

42. Agematu H, Matsumoto N, Fujii Y, Kabumoto H, Doi S, Machida K, Ishikawa J, Arisawa A (2006) Hydroxylation of testosterone by bacterial cytochromes P450 using the *Escherichia coli* expression system. Bioscience, Biotechnology & Biochemistry 70:307-11. https://doi.org/10.1271/bbb.70.307

43. Podust LM, Bach H, Kim Y, Lamb DC, Arase M, Sherman DH, Kelly SL, Waterman MR (2004) Comparison of the 1.85 Å structure of CYP154A1 from *Streptomyces coelicolor* A3(2) with the closely related CYP154C1 and CYPs from antibiotic biosynthetic pathways. Protein Science 13:255-68. https://doi.org/https://doi.org/10.1110/ps.03384804

44. Paudel P, Regmi KP, Kim K-H, Lee JH, Oh T-J (2024) Functional characterization and unraveling the structural determinants of novel steroid hydroxylase CYP154C7 from *Streptomyces* sp. PAMC26508. Heliyon 10:https://doi.org/10.1016/j.heliyon.2024.e39777

45. Herzog K, Bracco P, Onoda A, Hayashi T, Hoffmann K, Schallmey A (2014) Enzyme–substrate complex structures of CYP154C5 shed light on its mode of highly selective steroid hydroxylation. Acta Crystallographica 70:2875-89. https://doi.org/10.1107/S1399004714019129

46. Dangi B, Kim K-H, Kang S-H, Oh T-J (2018) Tracking down a new Steroid-hydroxylating promiscuous cytochrome P450: CYP154C8 from *Streptomyces* sp. W2233-SM. ChemBioChem 19:1066-77. https://doi.org/https://doi.org/10.1002/cbic.201800018

47. Makino T, Katsuyama Y, Otomatsu T, Misawa N, Ohnishi Y (2014) Regio- and stereospecific hydroxylation of various steroids at the 16α position of the D ring by the *Streptomyces griseus* cytochrome P450 CYP154C3. Applied and Environmental Microbiology 80:1371-9. https://doi.org/doi:10.1128/AEM.03504-13

48. Cheng Q, Lamb DC, Kelly SL, Lei L, Guengerich FP (2010) Cyclization of a cellular dipentaenone by *Streptomyces coelicolor* cytochrome P450 154A1 without oxidation/reduction. Journal of the American Chemical Society 132:15173-5. https://doi.org/10.1021/ja107801v

49. Von Bühler CJ, Urlacher VB (2014) A novel P450-based biocatalyst for the selective production of chiral 2-alkanols. Chemical Communications 50:4089. https://doi.org/10.1039/c4cc00647j

50. Schallmey A, den Besten G, Teune IGP, Kembaren RF, Janssen DB (2011) Characterization of cytochrome P450 monooxygenase CYP154H1 from the thermophilic soil bacterium *Thermobifida fusca*. Applied Microbiology and Biotechnology 89:1475-85. https://doi.org/10.1007/s00253-010-2965-9

51. Rühlmann A, Groth G, Urlacher VB (2018) Characterization of CYP154F1 from *Thermobifida fusca* YX and extension of Its substrate spectrum by site-directed mutagenesis. ChemBioChem 19:478-85. https://doi.org/https://doi.org/10.1002/cbic.201700565

52. Loomis CL, Brixius-Anderko S, Scott EE (2022) Redox partner adrenodoxin alters cytochrome P450 11B1 ligand binding and inhibition. Journal of Inorgorganic Biochememistry 235:111934. https://doi.org/10.1016/j.jinorgbio.2022.111934

53. Khatri Y, Schifrin A, Bernhardt R (2017) Investigating the effect of available redox protein ratios for the conversion of a steroid by a myxobacterial CYP260A1. FEBS Letters 591:1126-40. https://doi.org/https://doi.org/10.1002/1873-3468.12619

54. Tavanti M, Porter JL, Sabatini S, Turner NJ, Flitsch SL (2018) Panel of new thermostable CYP116B self-sufficient cytochrome P450 monooxygenases that

catalyze C−H activation with a diverse substrate scope. ChemCatChem 10:1042-51. https://doi.org/10.1002/cctc.201701510

55. Nguyen K-T, Nguyen N-L, Tung NV, Nguyen HH, Milhim M, Le T-T-X, Lai T-H-N, Phan T-T-M, Bernhardt R (2020) A Novel thermostable cytochrome P450 from sequence-based metagenomics of Binh Chau hot spring as a promising catalyst for testosterone conversion. Catalysts 10:1083. https://doi.org/10.3390/catal10091083

56. Koo LS, Tschirret-Guth RA, Straub WE, Moënne-Loccoz P, Loehr TM, Ortiz de Montellano PR (2000) The active site of the thermophilic CYP119 from *Sulfolobus solfataricus*. Journal of Biological Chemistry 275:14112-23. https://doi.org/https://doi.org/10.1074/jbc.275.19.14112

57. Oku Y, Ohtaki A, Kamitori S, Nakamura N, Yohda M, Ohno H, Kawarabayasi Y (2004) Structure and direct electrochemistry of cytochrome P450 from the thermoacidophilic crenarchaeon, *Sulfolobus tokodaii* strain 7. Journal of Inorganic Biochemistry 98:1194-9. https://doi.org/10.1016/j.jinorgbio.2004.05.002

58. Ho WW, Li H, Nishida CR, Ortiz de Montellano PR, Poulos TL (2008) Crystal structure and properties of CYP231A2 from the thermoacidophilic archaeon *Picrophilus torridus*. Biochemistry 47:2071-9. https://doi.org/10.1021/bi702240k

59. Kundral S, Giang PD, Grundon LR, Supper JM, Khare SK, Bernhardt PV, Evans P, Bell SG, De Voss JJ (2025) Characterisation of the thermophilic P450 CYP116B305 identified using metagenomics-derived sequence data from an Australian hot spring. Applied Microbiology and Biotechnology 109:https://doi.org/10.1007/s00253-025-13521-2

60. Mccarthy AJ, Cross T (1984) A taxonomic study of *Thermomonospora* and other monosporic actinomycetes. Microbiology 130:5-25. https://doi.org/https://doi.org/10.1099/00221287-130-1-5

61. Zhang Z, Wang Y, Ruan J (1998) Reclassification of *Thermomonospora* and *Microtetraspora*. International Journal of Systematic and Evolutionary Microbiology 48:411-22. https://doi.org/https://doi.org/10.1099/00207713-48-2-411

62. Bachmann S, L., McCarthy A, J. (1991) Purification and cooperative activity of enzymes constituting the xylan-degrading system of *Thermomonospora fusca*. Applied and Environmental Microbiology 57:2121-30. https://doi.org/10.1128/aem.57.8.2121-2130.1991

63. Zainudin MHM, Mustapha NA, Hassan MA, Bahrin EK, Tokura M, Yasueda H, Shirai Y (2019) A highly thermostable crude endoglucanase produced by a newly isolated *Thermobifida fusca* strain UPMC 901. Scientific Reports 9:https://doi.org/10.1038/s41598-019-50126-y

64. Lykidis A, Mavromatis K, Ivanova N, Anderson I, Land M, Dibartolo G, Martinez M, Lapidus A, Lucas S, Copeland A, Richardson P, Wilson DB, Kyrpides N (2007) Genome sequence and analysis of the soil cellulolytic actinomycete *Thermobifida fusca* YX. Journal of Bacteriology 189:2477-86. https://doi.org/10.1128/jb.01899-06

65. Podgorski MN, Coleman T, Chao RR, De Voss JJ, Bruning JB, Bell SG (2020) Investigation of the requirements for efficient and selective cytochrome P450 monooxygenase catalysis across different reactions. Journal of Inorganic Biochemistry 203:110913. https://doi.org/10.1016/j.jinorgbio.2019.110913

66. De Marco A (2013) Recombinant polypeptide production in *E. co*li: towards a rational approach to improve the yields of functional proteins. Microbial Cell Factories 12:101. https://doi.org/10.1186/1475-2859-12-101

67. Fazekas de St Groth S, Webster RG, Datyner A (1963) Two new staining procedures for quantitative estimation of proteins on electrophoretic strips. Biochimica et Biophysica Acta 71:377-91. https://doi.org/10.1016/0006-3002(63)91092-8

68. Barr I, Guo F (2015) Pyridine hemochromagen assay for determining the concentration of heme in purified protein solutions. Bio-protocol Journal 5:https://doi.org/10.21769/bioprotoc.1594

69. Grimsley GR, Pace CN (2004) Spectrophotometric determination of protein concentration. Current Protocols in Protein Science Chapter 3:3.1.-3.1.9. https://doi.org/10.1002/0471140864.ps0301s33

70. Erman JE, Kilheeney H, Bidwai AK, Ayala CE, Vitello LB (2013) Peroxygenase activity of cytochrome c peroxidase and three apolar distal heme pocket mutants: hydroxylation of 1-methoxynaphthalene. BMC Biochemistry 14:19. https://doi.org/10.1186/1471-2091-14-19

71. Kumwenda B, Litthauer D, Bishop ÖT, Reva O (2013) Analysis of protein thermostability enhancing factors in industrially iImportant *Thermus* bacteria species. Evolutionary Bioinformatics 9:327-43. https://doi.org/10.4137/ebo.s12539

72. Podgorski MN, Lee JHZ, Scaffidi-Muta JM, Akter J, Bell SG (2025) Characterisation of a self-sufficient cytochrome P450 enzyme from the bacterium *Thermosporothrix hazakensis* and its conversion into a peroxygenase. Microbial Biotechnology 18:e70234. https://doi.org/10.1111/1751-7915.70234

73. Omura T, Sato R (1964) The carbon monoxide-binding pigment of liver microsomes. I. evidence for its hemoprotein nature. Journal of Biological Chemistry 239:2370-8. https://www.ncbi.nlm.nih.gov/pubmed/14209971

74. Sabat J, Stuehr DJ, Yeh S-R, Rousseau DL (2009) Characterization of the proximal ligand in the P420 form of inducible nitric oxide synthase. Journal of the American Chemical Society 131:12186-92. https://doi.org/10.1021/ja901016a

75. Dunford AJ, McLean KJ, Sabri M, Seward HE, Heyes DJ, Scrutton NS, Munro AW (2007) Rapid P450 heme iron reduction by laser photoexcitation of *Mycobacterium tuberculosis* CYP121 and CYP51B1: analysis of co complexation reactions and reversibility of the P450/P420 equilibrium. Journal of Biological Chemistry 282:24816-24. https://doi.org/https://doi.org/10.1074/jbc.M702958200

76. McLean KJ, Cheesman MR, Rivers SL, Richmond A, Leys D, Chapman SK, Reid GA, Price NC, Kelly SM, Clarkson J, Smith WE, Munro AW (2002) Expression, purification and spectroscopic characterization of the cytochrome P450 CYP121 from *Mycobacterium tuberculosis*. Journal of Inorgorganic Biochemistry 91:527-41. https://doi.org/10.1016/s0162-0134(02)00479-8

77. Daff SN, Chapman SK, Turner KL, Holt RA, Govindaraj S, Poulos TL, Munro AW (1997) Redox control of the catalytic cycle of flavocytochrome P-450 BM3. Biochemistry 36:13816-23. https://doi.org/10.1021/bi971085s

78. Schenkman JB, Remmer H, Estabrook RW (1967) Spectral studies of drug interaction with hepatic microsomal cytochrome. Molecular Pharmacology 3:113-23.

79. Guengerich FP (1978) Destruction of heme and hemoproteins mediated by liver microsomal reduced nicotinamide adenine dinucleotide phosphate-cytochrome P-450 reductase. Biochemistry 17:3633-9. https://doi.org/10.1021/bi00610a033

80. Albertolle ME, Kim D, Nagy LD, Yun C-H, Pozzi A, Savas Ü, Johnson EF, Guengerich FP (2017) Heme–thiolate sulfenylation of human cytochrome P450 4A11 functions as a redox switch for catalytic inhibition. Journal of Biological Chemistry 292:11230-42. https://doi.org/10.1074/jbc.m117.792200

81. Dezvarei S, Shoji O, Watanabe Y, Bell SG (2019) The effect of decoy molecules on the activity of the P450Bm3 holoenzyme and a heme domain peroxygenase variant. Catalysis Communications 124:97-102. https://doi.org/https://doi.org/10.1016/j.catcom.2019.03.004

82. Munday SD, Dezvarei S, Bell SG (2016) Increasing the activity and efficiency of stereoselective oxidations by using decoy molecules in combination with rate-enhancing variants of P450Bm3. ChemCatChem 8:2789-96. https://doi.org/https://doi.org/10.1002/cctc.201600551

83. Roiban GD, Agudo R, Ilie A, Lonsdale R, Reetz MT (2014) CH-activating oxidative hydroxylation of 1-tetralones and related compounds with high regio- and stereoselectivity. Chemical Communications 50:14310-3. https://doi.org/10.1039/c4cc04925j

84. Whitehouse CJC, Bell SG, Wong L-L (2008) Desaturation of alkylbenzenes by cytochrome P450BM3 (CYP102A1). Chemistry – A European Journal 14:10905-8. https://doi.org/https://doi.org/10.1002/chem.200801927

85. Lai W, Chen H, Cohen S, Shaik S (2011) Will P450cam hydroxylate or desaturate alkanes? QM and QM/MM studies. The Journal of Physical Chemistry Letters 2:2229-35. https://doi.org/10.1021/jz2007534

86. Miettinen K, Dong L, Navrot N, Schneider T, Burlat V, Pollier J, Woittiez L, van der Krol S, Lugan R, Ilc T, Verpoorte R, Oksman-Caldentey K-M, Martinoia E, Bouwmeester H, Goossens A, Memelink J, Werck-Reichhart D (2014) The seco-iridoid pathway from *Catharanthus roseus*. Nature Communications 5:3606. https://doi.org/10.1038/ncomms4606

87. Fansher DJ, Besna JN, Fendri A, Pelletier JN (2024) Choose your own adventure: a comprehensive database of reactions catalyzed by cytochrome P450 BM3 variants. ACS Catalysis 14:5560-92. https://doi.org/10.1021/acscatal.4c00086

88. Shoji O, Wiese C, Fujishiro T, Shirataki C, Wünsch B, Watanabe Y (2010) Aromatic C–H bond hydroxylation by P450 peroxygenases: a facile colorimetric assay for monooxygenation activities of enzymes based on Russig's blue formation. Journal of Biological Inorganic Chemistry 15:1109-15. https://doi.org/10.1007/s00775-010-0671-9

89. Ullrich R, Poraj-Kobielska M, Herold-Majumdar OM, Vind J, Hofrichter M (2021) Synthesis of indigo-dyes from indole derivatives by unspecific peroxygenases and their application for *in-situ* dyeing. Catalysts 11:1495. https://www.mdpi.com/2073-4344/11/12/1495

90. Fabara AN, Fraaije MW (2020) An overview of microbial indigo-forming enzymes. Applied Microbiology and Biotechnology 104:925-33. https://doi.org/10.1007/s00253-019-10292-5

91. Ma L, Sun T, Liu Y, Zhao Y, Liu X, Li Y, Chen X, Cao L, Kang Q, Guo J, Du L, Wang W, Li S (2023) Enzymatic synthesis of indigo derivatives by tuning P450 BM3 peroxygenases. Synthetic and Systems Biotechnology 8:452-61. https://doi.org/https://doi.org/10.1016/j.synbio.2023.06.006

92. Fansher DJ, Besna JN, Pelletier JN (2024) Indigo production identifies hotspots in cytochrome P450 BM3 for diversifying aromatic hydroxylation. Faraday Discuss 252:29-51. https://doi.org/10.1039/d4fd00017j

93. Whitehouse CJ, Bell SG, Tufton HG, Kenny RJ, Ogilvie LC, Wong LL (2008) Evolved CYP102A1 (P450BM3) variants oxidise a range of non-natural substrates and offer new selectivity options. Chemical Commununications, 966-8. https://doi.org/10.1039/b718124h

94. Oelgemöller M, Mattay J, Görner H (2010) Direct photooxidation and xanthene-ensitized oxidation of naphthols: quantum yields and mechanism. The Journal of Physical Chemistry A 115:280-5. https://doi.org/10.1021/jp108832x

95. Barrios DA, D'Antonio J, McCombs NL, Zhao J, Franzen S, Schmidt AC, Sombers LA, Ghiladi RA (2014) Peroxygenase and oxidase activities of dehaloperoxidase-hemoglobin from *Amphitrite ornata*. J Am Chem Soc 136:7914-25. https://doi.org/10.1021/ja500293c

96. Deutsch JC (1998) Ascorbic acid oxidation by hydrogen peroxide. Analytical Biochemistry 255:1-7. https://doi.org/https://doi.org/10.1006/abio.1997.2293

97. Scandurra R, Consalvi V, Chiaraluce R, Politi L, Engel PC (1998) Protein thermostability in extremophiles. Biochimie 80:933-41. https://doi.org/10.1016/S0300-9084(00)88890-2

98. Gee AR, Stone ISJ, Stockdale TP, Pukala TL, De Voss JJ, Bell SG (2023) Efficient biocatalytic C–H bond oxidation: an engineered heme-thiolate peroxygenase from a thermostable cytochrome P450. Chemical Communications 59:13486-9. https://doi.org/10.1039/D3CC04626E

99. McLean MA, Maves SA, Weiss KE, Krepich S, Sligar SG (1998) Characterization of a cytochrome P450 from the acidothermophilic archaea *Sulfolobus solfataricus*. Biochemical and Biophysical Research Communications 252:166-72. https://doi.org/https://doi.org/10.1006/bbrc.1998.9584

100. Blasco F, Kauffmann I, Schmid RD (2004) CYP175A1 from *Thermus thermophilus* HB27, the first β-carotene hydroxylase of the P450 superfamily. Applied Microbiology and Biotechnology 64:671-4. https://doi.org/10.1007/s00253-003-1529-7

101. Yano JK, Blasco F, Li H, Schmid RD, Henne A, Poulos TL (2003) Preliminary characterization and crystal structure of a thermostable cytochrome P450 from *Thermus thermophilus* Journal of Biological Chemistry 278:608-16. https://doi.org/https://doi.org/10.1074/jbc.M206568200

102. Abramson J, Adler J, Dunger J, Evans R, Green T, Pritzel A, Ronneberger O, Willmore L, Ballard AJ, Bambrick J, Bodenstein SW, Evans DA, Hung C-C, O'Neill M, Reiman D, Tunyasuvunakool K, Wu Z, Žemgulytė A, Arvaniti E, Beattie C, Bertolli O, Bridgland A, Cherepanov A, Congreve M, Cowen-Rivers AI, Cowie A, Figurnov M, Fuchs FB, Gladman H, Jain R, Khan YA, Low CMR, Perlin K, Potapenko A, Savy P, Singh S, Stecula A, Thillaisundaram A, Tong C, Yakneen S, Zhong ED, Zielinski M, Žídek A, Bapst V, Kohli P, Jaderberg M, Hassabis D, Jumper JM (2024) Accurate structure prediction of biomolecular interactions with AlphaFold 3. Nature 630:493-500. https://doi.org/10.1038/s41586-024-07487-w

103. Fujitsu H, Shirahama S, Matsumura E, Takeshita K, Mochida I (1981) Catalytic hydrogenation of styrene oxide with cationic rhodium complexes. The Journal of Organic Chemistry 46:2287-90. https://doi.org/10.1021/jo00324a016

104. Yadav GD, Lawate YS (2013) Hydrogenation of styrene oxide to 2-phenyl ethanol over polyurea microencapsulated mono- and bimetallic nanocatalysts: activity, selectivity, and kinetic modeling. Industrial & Engineering Chemistry Research 52:4027-39. https://doi.org/10.1021/ie302587j

105. Chua LS, Sarmidi MR (2004) Immobilised lipase-catalysed resolution of (R,S)-1-phenylethanol in recirculated packed bed reactor. Journal of Molecular Catalysis B: Enzymatic 28:111-9. https://doi.org/https://doi.org/10.1016/j.molcatb.2004.02.004

106. Khetmalis YM, Shivani M, Murugesan S, Chandra Sekhar KVG (2021) Oxindole and its derivatives: a review on recent progress in biological activities. Biomedicine & Pharmacotherapy 141:111842. https://doi.org/10.1016/j.biopha.2021.111842

107. Kaur M, Singh M, Chadha N, Silakari O (2016) Oxindole: a chemical prism carrying plethora of therapeutic benefits. European Journal of Medicinal Chemistry 123:858-94. https://doi.org/https://doi.org/10.1016/j.ejmech.2016.08.011

108. Daloze D, Pasteels JM (1994) Isolation of 8-hydroxygeraniol-8-O-β-d-glucoside, a probable intermediate in biosynthesis of iridoid monoterpenes, from defensive secretions of P*lagiodera versicolora* and G*astrophysa viridula* (*Coleoptera*: *Chrysomelidae*). Journal of Chemical Ecology 20:2089-97. https://doi.org/10.1007/BF02066245

109. Wang H, Jiang G, Liang N, Dong T, Shan M, Yao M, Wang Y, Xiao W, Yuan Y (2023) Systematic engineering to enhance 8-hydroxygeraniol production in yeast. Journal of Agricultural and Food Chemistry 71:4319-27. https://doi.org/10.1021/acs.jafc.2c09028

Supplementary Files

This is a list of supplementary files associated with this preprint. Click to download.

- SIversion2.pdf